PAPER • OPEN ACCESS

Overview of the EUROfusion Tokamak Exploitation programme in support of ITER and DEMO

To cite this article: E. Joffrin *et al* 2024 *Nucl. Fusion* **64** 112019

View the article online for updates and enhancements.

Overview of the EUROfusion Tokamak Exploitation programme in support of ITER and DEMO

E. Joffrin[1,*] , M. Wischmeier[2], M. Baruzzo[3], A. Hakola[4], A. Kappatou[2] , D. Keeling[5],
B. Labit[6] , E. Tsitrone[1], N. Vianello[3] , the ASDEX Upgrade Team[a], JET Contributors[b],
the MAST-U Team[c], the TCV Team[d], the WEST Team[e], the EUROfusion Tokamak
Exploitation Team: D. Abate[7], J. Adamek[9], M. Agostini[7], C. Albert[10], F.C.P. Albert
Devasagayam[11], S. Aleiferis[5], E. Alessi[12], J. Alhage[13], S. Allan[5], J. Allcock[5], M. Alonzo[3],
G. Anastasiou[14], E. Andersson Sunden[15], C. Angioni[2], Y. Anquetin[16], L. Appel[5],
G.M. Apruzzese[3], M. Ariola[17], C. Arnas[18], J.F. Artaud[1], W. Arter[5], O. Asztalos[19],
L. Aucone[20], M.H. Aumeunier[1], F. Auriemma[7], J. Ayllon[41], E. Aymerich[21], A. Baciero[22],
F. Bagnato[6], L. Bähner[23], F. Bairaktaris[14], P. Balázs[19], L. Balbinot[7], I. Balboa[5], M. Balden[2],
A. Balestri[6], M. Baquero Ruiz[6], T. Barberis[24], C. Barcellona[25], O. Bardsley[5], M. Baruzzo[3],
S. Benkadda[16], T. Bensadon[48], E. Bernard[1], M. Bernert[2], H. Betar[26], R. Bianchetti Morales[5],
J. Bielecki[27], R. Bilato[2], P. Bilkova[9], W. Bin[12], G. Birkenmeier[2], R. Bisson[18], P. Blanchard[6],
A. Bleasdale[5], V. Bobkov[2], A. Boboc[5], A. Bock[2], K. Bogar[9], P. Bohm[9], T. Bolzonella[7],
F. Bombarda[3], N. Bonanomi[2], L. Boncagni[3], D. Bonfiglio[7], R. Bonifetto[24], M. Bonotto[7],
D. Borodin[28], I. Borodkina[9], T.O.S.J. Bosman[29], C. Bourdelle[1], C. Bowman[5],
S. Brezinsek[28,76], D. Brida[2], F. Brochard[30], R. Brunet[1], D. Brunetti[5], V. Bruno[1],
R. Buchholz[10], J. Buermans[31], H. Bufferand[1], P. Buratti[3], A. Burckhart[2], J. Cai[28],
R. Calado[32], J. Caloud[9], S. Cancelli[20], F. Cani[33], B. Cannas[21], M. Cappelli[3], S. Carcangiu[21],
A. Cardinali[3], S. Carli[34], D. Carnevale[35], M. Carole[16], M. Carpita[6], D. Carralero[22],
F. Caruggi[20], I.S. Carvalho[5,36], I. Casiraghi[12], A. Casolari[9], F.J. Casson[5], C. Castaldo[3],
A. Cathey[2], F. Causa[12], J. Cavalier[9], M. Cavedon[20], J. Cazabonne[6], M. Cecconello[15],
L. Ceelen[29], A. Celora[20], J. Cerovsky[9], C.D. Challis[5], R. Chandra[11], A. Chankin[2],
B. Chapman[5], H. Chen[41], M. Chernyshova[37], A.G. Chiariello[17], P. Chmielewski[37],
A. Chomiczewska[37], C. Cianfarani[3], G. Ciraolo[1], J. Citrin[29], F. Clairet[1], S. Coda[6],
R. Coelho[32], J.W. Coenen[28], I.H. Coffey[38], C. Colandrea[6], L. Colas[1], S. Conroy[15],
C. Contre[6], N.J. Conway[5], L. Cordaro[7], Y. Corre[1], D. Costa[32], S. Costea[39], D. Coster[2],
X. Courtois[1], C. Cowley[40], T. Craciunescu[42], G. Croci[20], A.M. Croitoru[42], K. Crombe[31],
D.J. Cruz Zabala[41], G. Cseh[19], T. Czarski[37], A. Da Ros[1], A. Dal Molin[20], M. Dalla Rosa[20],
Y. Damizia[5], O. D'Arcangelo[3], P. David[2], M. De Angeli[12], E. De la Cal[22], E. De La Luna[22],
G. De Tommasi[17], J. Decker[6], R. Dejarnac[9], D. Del Sarto[26], G. Derks[29], C. Desgranges[1],
P. Devynck[1], S. Di Genova[43], L.E. di Grazia[17], A. Di Siena[2], M. Dicorato[16], M. Diez[1],
M. Dimitrova[9], T. Dittmar[28], L. Dittrich[23], J.J. Domínguez Palacios Durán[41], P. Donnel[1],
D. Douai[1], S. Dowson[5], S. Doyle[41], M. Dreval[44], P. Drews[28], L. Dubus[1], R. Dumont[1],

---

D. Dunai[19], M. Dunne[2], A. Durif[1], F. Durodie[31], G. Durr Legoupil Nicoud[6], B. Duval[6],
R. Dux[2], T. Eich[2], A. Ekedahl[1], S. Elmore[5], G. Ericsson[15], J. Eriksson[15], B. Eriksson[15],
F. Eriksson[5], S. Ertmer[28], A. Escarguel[18], B. Esposito[3], T. Estrada[22], E. Fable[2], M. Faitsch[2],
N. Fakhrayi Mofrad[11], A. Fanni[21], T. Farley[5], M. Farník[9], N. Fedorczak[1], F. Felici[6], X. Feng[45],
J. Ferreira[32], D. Ferreira[32], N. Ferron[7], O. Fevrier[6], O. Ficker[9], A.R. Field[5], A. Figueiredo[32],
N. Fil[5], D. Fiorucci[3], M. Firdaouss[1], R. Fischer[2], M. Fitzgerald[5], M. Flebbe[28], M. Fontana[5],
J. Fontdecaba Climent[22], A. Frank[6], E. Fransson[46], L. Frassinetti[23], D. Frigione[35],
S. Futatani[48], R. Futtersack[5], S. Gabriellini[47], D. Gadariya[22], D. Galassi[6], K. Galazka[37],
J. Galdon[41], S. Galeani[35], D. Gallart[48], A. Gallo[1], C. Galperti[6], M. Gambrioli[7],
S. Garavaglia[12], J. Garcia[1], M. Garcia Munoz[41], J. Gardarein[16], L. Garzotti[5],
J. Gaspar[49], R. Gatto[47], P. Gaudio[35], M. Gelfusa[35], J. Gerardin[1], S.N. Gerasimov[5],
R. Gerru Miguelanez[50], G. Gervasini[12], Z. Ghani[5], F.M. Ghezzi[12], G. Ghillardi[3],
L. Giannone[2], S. Gibson[5], L. Gil[32], A. Gillgren[46], E. Giovannozzi[3], C. Giroud[5], G. Giruzzi[1],
T. Gleiter[2], M. Gobbin[7], V. Goloborodko[51], A. González Ganzábal[22], T. Goodman[6],
V. Gopakumar[5], G. Gorini[20], T. Görler[2], S. Gorno[6], G. Granucci[12], D. Greenhouse[40],
G. Grenfell[2], M. Griener[2], W. Gromelski[37], M. Groth[11], O. Grover[2,9], M. Gruca[37], A. Gude[2],
C. Guillemaut[1], R. Guirlet[1], J. Gunn[1], T. Gyergyek[39], L. Hagg[15], A. Hakola[4], J. Hall[13],
C.J. Ham[5], M. Hamed[29], T. Happel[2], G. Harrer[52], J. Harrison[5], D. Harting[28], N.C. Hawkes[5],
P. Heinrich[2], S. Henderson[5], P. Hennequin[53], R. Henriques[5], S. Heuraux[30],
J. Hidalgo Salaverri[41], J. Hillairet[1], J.C. Hillesheim[5], A. Hjalmarsson[15], A. Ho[29], J. Hobirk[2],
E. Hodille[1], M. Hölzl[2], M. Hoppe[6,23], J. Horacek[9], N. Horsten[34], L. Horvath[5], M. Houry[1],
K. Hromasova[9], J. Huang[28], Z. Huang[5], A. Huber[28], E. Huett[6], P. Huynh[1], A. Iantchenko[6],
M. Imrisek[9], P. Innocente[7], C. Ionita Schrittwieser[54], H. Isliker[58], P. Ivanova[55],
I. Ivanova Stanik[37], M. Jablczynska[37], S. Jachmich[36], A.S. Jacobsen[50], P. Jacquet[5],
A. Jansen van Vuuren[6,41], A. Jardin[56], H. Järleblad[50], A. Järvinen[4], F. Jaulmes[9],
T. Jensen[50], I. Jepu[5,42], S. Jessica[57], E. Joffrin[1], T. Johnson[23], A. Juven[1], J. Kalis[2],
A. Kappatou[2], J. Karhunen[4], R. Karimov[6], A.N. Karpushov[6], S. Kasilov[10], Y. Kazakov[31],
P.V. Kazantzidis[14], D. Keeling[5], W. Kernbichler[10], HT. Kim[5], D.B. King[5], V.G. Kiptily[5],
A. Kirjasuo[4], K.K. Kirov[5], A. Kirschner[28], A. Kit[59], T. Kiviniemi[11], F. Kjær[50], E. Klinkby[50],
A. Knieps[28], U. Knoche[28], M. Kochan[36], F. Köchl[5], G. Kocsis[5], J.T.W. Koenders[29], L. Kogan[5],
Y. Kolesnichenko[51], Y. Kominis[14], M. Komm[9], M. Kong[6], B. Kool[29], S.B. Korsholm[50],
D. Kos[5], M. Koubiti[16], J. Kovacic[39], Y. Kovtun[44], E. Kowalska Strzeciwilk[37], K. Koziol[60],
M. Kozulia[44], A. Krämer Flecken[28], A. Kreter[28], K. Krieger[2], U. Kruezi[36], O. Krutkin[6],
O. Kudlacek[2], U. Kumar[6], H. Kumpulainen[11], M.H. Kushoro[20], R. Kwiatkowski[60],
M. La Matina[7], B. Labit[6], M. Lacquaniti[21], L. Laguardia[12], P. Lainer[10], P. Lang[2], M. Larsen[50],
E. Laszynska[37], K.D. Lawson[5], A. Lazaros[14], E. Lazzaro[12], M.Y.K. Lee[6], S. Leerink[11],
M. Lehnen[36], M. Lennholm[5], E. Lerche[31], Y. Liang[28], A. Lier[2], J. Likonen[4], O. Linder[2],
B. Lipschultz[40], A. Listopad[6], X. Litaudon[1], E. Litherland Smith[5], D. Liuzza[3], T. Loarer[1],
P.J. Lomas[5], J. Lombardo[7], N. Lonigro[40], R. Lorenzini[7], C. Lowry[5], T. Luda di Cortemiglia[2],
A. Ludvig Osipov[46], T. Lunt[2], V. Lutsenko[51], E. Macusova[9], R. Mäenpää[11], P. Maget[1],
C.F. Maggi[5], J. Mailloux[5], S. Makarov[2], K. Malinowski[37], P. Manas[1], A. Mancini[41],
D. Mancini[6,33], P. Mantica[33], M. Mantsinen[61], J. Manyer[48], M. Maraschek[2], G. Marceca[6],
G. Marcer[12], C. Marchetto[62], S. Marchioni[6], A. Mariani[12], M. Marin[6], M. Markl[10],
T. Markovic[9], D. Marocco[3], S. Marsden[5], L. Martellucci[35], P. Martin[7], C. Martin[18],
F. Martinelli[35], L. Martinelli[6], J.R. Martin Solis[63], R. Martone[17], M. Maslov[5], R. Masocco[35],
M. Mattei[17], G.F. Matthews[5], D. Matveev[28], E. Matveeva[9], M.L. Mayoral[5], D. Mazon[1],
S. Mazzi[6,16], C. Mazzotta[3], G. McArdle[5], R. McDermott[2], K. McKay[41], A.G. Meigs[5],
C. Meineri[24], A. Mele[33], V. Menkovski[64], S. Menmuir[5], A. Merle[6], H. Meyer[5],
K. Mikszuta Michalik[37], D. Milanesio[24], F. Militello[5], A. Milocco[20], I.G. Miron[42], J. Mitchell[5],
R. Mitteau[1], V. Mitterauer[2], J. Mlynar[9], V. Moiseenko[44], P. Molna[6], F. Mombelli[65], C. Monti[3],
A. Montisci[21], J. Morales[1], P. Moreau[1], J.M. Moret[6], A. Moro[12], D. Moulton[5],

P. Mulholland[64], M. Muraglia[16], A. Murari[7], A. Muraro[12], P. Muscente[7], D. Mykytchuk[6],
F. Nabais[32], Y. Nakeva[33], F. Napoli[3], E. Nardon[1], M.F. Nave[32], R.D. Nem[50], A. Nielsen[50],
S.K. Nielsen[50], M. Nocente[20], R. Nouailletas[1], S. Nowak[12], H. Nyström[23], R. Ochoukov[2],
N. Offeddu[6], S. Olasz[19], C. Olde[5], F. Oliva[35], D. Oliveira[6], H.J.C. Oliver[5], P. Ollus[11],
J. Ongena[31], F.P. Orsitto[3], N. Osborne[5], R. Otin[5], P. Oyola Dominguez[41], D.I. Palade[42],
S. Palomba[35], O. Pan[2], N. Panadero[22], E. Panontin[20], A. Papadopoulos[14], P. Papagiannis[14],
G. Papp[2], V.V. Parail[5], C. Pardanaud[16], J. Parisi[66], A. Parrott[5], K. Paschalidis[67],
M. Passoni[65], F. Pastore[6], A. Patel[5], B. Patel[5], A. Pau[6], G. Pautasso[2], R. Pavlichenko[44],
E. Pawelec[60], B. Pegourie[1], G. Pelka[37], E. Peluso[35], A. Perek[6,29], E. Perelli Cippo[12],
C. Perez Von Thun[37], P. Petersson[23], G. Petravich[19], Y. Peysson[1], V. Piergotti[3], L. Pigatto[7],
C. Piron[3], L. Piron[7], A. Pironti[17], F. Pisano[21], U. Plank[2], B. Ploeckl[2], V. Plyusnin[32],
A. Podolnik[9], Y. Poels[6,64], G. Pokol[19], J. Poley[6], G. Por[19], M. Poradzinski[5], F. Porcelli[24],
L. Porte[6], C. Possieri[35], A. Poulsen[50], I. Predebon[7], G. Pucella[3], M. Pueschel[29], P. Puglia[6],
O. Putignano[20], T. Pütterich[2], V. Quadri[1], A. Quercia[17], M. Rabinski[60], L. Radovanovic[52],
R. Ragona[50], H. Raj[6], M. Rasinski[28], J. Rasmussen[50], G. Ratta[22], S. Ratynskaia[67],
R. Rayaprolu[28], M. Rebai[12], A. Redl[33], D. Rees[11], D. Refy[19], M. Reich[2], H. Reimerdes[6],
B.C.G. Reman[50], O. Renders[34], C. Reux[1], D. Ricci[12], M. Richou[1], S. Rienacker[53],
D. Rigamonti[12], F. Rigollet[68], F.G. Rimini[5,69], D. Ripamonti[12], N. Rispoli[12], N. Rivals[1],
J.F. Rivero Rodriguez[41], C. Roach[5], G. Rocchi[3], S. Rode[28,76], P. Rodrigues[32],
J. Romazanov[28], C.F. Romero Madrid[41], J. Rosato[16], R. Rossi[35], G. Rubino[3],
J. Rueda Rueda[41], J. Ruiz Ruiz[66], P. Ryan[5], D. Ryan[5], S. Saarelma[5], R. Sabot[1],
M. Salewski[50], A. Salmi[4], L. Sanchis[11], A. Sand[11], J. Santos[32], K. Särkimäki[2], M. Sassano[35],
O. Sauter[6], G. Schettini[70], S. Schmuck[12], P. Schneider[2], N. Schoonheere[1], R. Schramm[2],
R. Schrittwieser[54], C. Schuster[2], N. Schwarz[2], F. Sciortino[2], M. Scotto D'Abusco[1],
S. Scully[5], A. Selce[12], L. Senni[3], M. Senstius[50], G. Sergienko[28], S.E. Sharapov[5],
R. Sharma[5], A. Shaw[5], U. Sheikh[6], G. Sias[21], B. Sieglin[2], S.A. Silburn[5], C. Silva[32],
A. Silva[32], D. Silvagni[2], B. Simmendefeldt Schmidt[50], L. Simons[6], J. Simpson[5], L. Singh[24],
S. Sipilä[11], Y. Siusko[44], S. Smith[5], A. Snicker[4], E.R. Solano[22], V. Solokha[11], M. Sos[9],
C. Sozzi[12], F. Spineanu[42], G. Spizzo[7], M. Spolaore[7], L. Spolladore[35], C. Srinivasan[5],
A. Stagni[7], Z. Stancar[5], G. Stankunas[71], J. Stober[2], P. Strand[46], C.I. Stuart[5], F. Subba[24],
G.Y. Sun[6], H.J. Sun[5], W. Suttrop[2], J. Svoboda[9], T. Szepesi[19], G. Szepesi[5], B. Tal[2], T. Tala[4],
P. Tamain[1], G. Tardini[2], M. Tardocchi[12], D. Taylor[5], G. Telesca[37], A. Tenaglia[35], A. Terra[28],
D. Terranova[7], D. Testa[6], C. Theiler[6], E. Tholerus[5], B. Thomas[5], E. Thoren[67], A. Thornton[5],
A. Thrysoe[50], Q. TICHIT[1], W. Tierens[2], A. Titarenko[72], P. Tolias[67], E. Tomasina[7], M. Tomes[9],
E. Tonello[6,65], A. Tookey[5], M. Toscano Jiménez[41], C. Tsironis[14], E. Tsitrone[1], E. Tsitrone[1],
C. Tsui[6,73], A. Tykhyy[51], M. Ugoletti[7], M. Usoltseva[2], D.F. Valcarcel[5], A. Valentini[50],
M. Valisa[7], M. Vallar[6], M. Valovic[5], Sl. Valvis[14], M. van Berkel[29], D. Van Eester[31],
S. Van Mulders[6], M. van Rossem[6], R. Vann[40], B. Vanovac[74], J. Varela Rodriguez[63],
J. Varje[11], S. Vartanian[1], M. Vecsei[19], L. Velarde Gallardo[41], M. Veranda[7], T. Verdier[50],
G. Verdoolaege[13], K. Verhaegh[5], L. Vermare[53], G. Verona Rinati[35], N. Vianello[7,8],
J. Vicente[32], E. Viezzer[41], L. Vignitchouk[67], F. Villone[17], B. Vincent[6], P. Vincenzi[7],
M.O. Vlad[42], G. Vogel[2], I. Voitsekhovitch[5], I. Voldiner[22], P. Vondracek[9], N.M.T. VU[6],
T. Vuoriheimo[59], C. Wade[45], E. Wang[28], T. Wauters[36], M. Weiland[2], H. Weisen[6,72],
N. Wendler[37], D. Weston[5], A. Widdowson[5], S. Wiesen[28], M. Wiesenberger[50], T. Wijkamp[64],
M. Willensdorfer[2], T. Wilson[5], M. Wischmeier[2], A. Wojenski[75], C. Wuethrich[6], I. Wyss[35],
L. Xiang[5], S. Xu[28], D. Yadykin[46], Y. Yakovenko[51], H. Yang[1], V. Yanovskiy[9], R. Yi[28], B. Zaar[23],
G. Zadvitskiy[9], L. Zakharov[59], P. Zanca[7], D. Zarzoso[16], Y. Zayachuk[5], J. Zebrowski[60],
M. Zerbini[3], P. Zestanakis[14], C. F. B. Zimmermann[2], M. Zlobinski[28], A. Zohar[39], V.K. Zotta[47],
X. Zou[1], M. Zuin[7], M. Zurita[6], I. Zychor[60]

[1] IRFM-CEA Centre de Cadarache, 13108 Sant-Paul-lez-Durance, France

[2] Max Planck Institute for Plasma Physics, Boltzmannstrasse 2, 85748 Garching bei München, Germany

[3] Dip.to Fusione e Tecnologie per la Sicurezza Nucleare, ENEA C. R. Frascati, via E. Fermi 45, 00044 Frascati (Roma), Italy

[4] VTT Technical Research Centre of Finland, PO Box 1000, FIN-02044 VTT, Espoo Finland

[5] United Kingdom Atomic Energy Authority, Culham Science Centre, Abingdon, Oxfordshire OX14 3DB, United Kingdom of Great Britain and Northern Ireland

[6] École Polytechnique Fédérale de Lausanne (EPFL), Swiss Plasma Center (SPC), CH-1015 Lausanne, Switzerland

[7] Consorzio RFX (CNR, ENEA, INFN, University of Padova, Acciaierie Venete SpA), C.so Stati Uniti 4, 35127 Padova, Italy

[8] Istituto per la Scienza e la Tecnologia dei Plasmi, CNR, Padova, Italy

[9] Institute of Plasma Physics of the CAS, Za Slovankou 1782/3, 182 00 Praha 8, Praha as indicated Czech Republic

[10] Graz University of Technology, Petersgasse 16, 8010 Graz, Austria

[11] Aalto University, PO Box 14100, FIN-00076 Aalto, Finland

[12] Institute for Plasma Science and Technology, CNR, via R. Cozzi 53, 20125 Milano, Italy

[13] Department of Applied Physics, Ghent University, 9000 Ghent, Belgium

[14] National Technical University of Athens, Iroon Politechniou 9, 157 73 Zografou, Athens, Greece

[15] Department of Physics and Astronomy, Uppsala University, SE-75120 Uppsala, Sweden

[16] Aix-Marseille University, CNRS, PIIM, UMR 7345, 13013 Marseille, France

[17] Consorzio CREATE, Via Claudio 21, 80125 Napoli, Italy

[18] Aix Marseille University, CNRS, PIIM, F-13397 Marseille CEDEX 20, France

[19] Centre for Energy Research, POB 49, H-1525 Budapest, Hungary

[20] University of Milano-Bicocca, Piazza della Scienza 3, 20126 Milano, Italy

[21] Department of Electrical and Electronic Engineering, University of Cagliari, Italy

[22] Laboratorio Nacional de Fusión, CIEMAT, Cagliari 28040 Madrid, Spain

[23] Electromagnetic Engineering and Fusion Science, EECS, KTH Royal Institute of Technology, Stockholm as indicated. SE-10044 Stockholm, Sweden

[24] Politecnico di Torino, Corso Duca degli Abruzzi, 24, 10129 Torino, Italy

[25] Dipartimento di Ingegneria Elettrica Elettronica e Informatica, Università degli Studi di Catania, 95125 Catania, Italy

[26] Institut Jean Lamour, UMR 7198, CNRS-Université de Lorraine, 54500 Vandoeuvre-lès-Nancy, France

[27] Institute of Nuclear Physics, Radzikowskiego 152, 31-342 Kraków, Poland

[28] Forschungszentrum Jülich GmbH, Institut für Energie- und Klimaforschung, Plasmaphysik, 52425 Jülich, Germany

[29] DIFFER-Dutch Institute for Fundamental Energy Research, Eindhoven, Netherlands

[30] Institut Jean Lamour, Université de Lorraine, Nancy, France

[31] Laboratory for Plasma Physics LPP-ERM/KMS, B-1000 Brussels, Belgium

[32] Instituto de Plasmas e Fusão Nuclear, Instituto Superior Técnico, Universidade de Lisboa, 1049-001 Lisboa, Portugal

[33] DEIM Department, Universitá degli Studi della Tuscia, Viterbo, Italy

[34] Department of Mechanical Engineering, KU Leuven, Leuven, Belgium

[35] Università di Roma Tor Vergata, Via del Politecnico 1, Roma, Italy

[36] ITER Organization, Route de Vinon-sur-Verdon, CS 90 046, 13067 Saint Paul Lez Durance Cedex, France

[37] Institute of Plasma Physics and Laser Microfusion, Hery 23, 01-497 Warsaw, Poland

[38] Astrophysics Research Centre, School of Mathematics and Physics, Queen's University, Belfast BT7 1NN, United Kingdom of Great Britain and Northern Ireland

[39] Jožef Stefan Institute, Ljubljana, Slovenia–University of Ljubljana, Lyubljana, Slovenia

[40] York Plasma Institute, Department of Physics, University of York, York YO10 5DD, United Kingdom of Great Britain and Northern Ireland

[41] Universidad de Sevilla, Sevilla, Spain

[42] The National Institute for Laser, Plasma and Radiation Physics, Magurele-Bucharest, Romania

[43] Aix-Marseille University, CNRS, M2P2, Marseille, France

[44] National Science Center Kharkov Institute of Physics and Technology, Akademichna 1, Kharkiv 61108, Ukraine

[45] Department of Physics, Durham University, Durham DH1 3LE, United Kingdom of Great Britain and Northern Ireland

[46] Department of Space, Earth and Environment, SEE, Chalmers University of Technology, SE-41296 Gothenburg, Sweden

[47] Dipartimento di Ingegneria Astronautica, Elettrica ed Energetica, SAPIENZA Università di Roma, Via Eudossiana 18, 00184 Roma, Italy

[48] Barcelona Supercomputing Center, Barcelona, Spain

[49] Aix-Marseille University, CNRS, IUSTI, UMR 7343, 13013 Marseille, France

[50] Department of Physics, Technical University of Denmark, Bldg 309, DK-2800 Kgs Lyngby, Denmark

[51] Institute for Nuclear Research, Prospekt Nauky 47, Kyiv 03680, Ukraine

[52] Technische Universität Wien, Wiedner Hauptstr. 8-10/134, A-1040 Wien, Austria

[53] Laboratoire de Physique des Plasmas, Ecole Polytechnique, Palaiseau, France

[54] Institute of Ion Physics and Applied Physics, University of Innsbruck, Innsbruck Austria

[55] Institute of Electronics, Bulgarian Academy of Sciences (BAS), 72 Tsarigradsko Chaussee, 1784 Sofia, Bulgaria

[56] Institute of Nuclear Physics Polish Academy of Sciences (IFJ PAN), Krakow, Poland

[57] Loughborough University, Loughborough, Leicestershire, United Kingdom of Great Britain and Northern Ireland

[58] Section of Astrophysics, Astronomy and Mechanics, Physics Department, Aristotle University, Thessaloniki GR 541 24, Greece

[59] University of Helsinki, PO Box 43, FI-00014 University of Helsinki, Helsinki Finland

[60] National Centre for Nuclear Research (NCBJ), 05-400 Otwock-Świerk, Poland

[61] ICREA and Barcelona Supercomputing Center, Barcelona, Spain

[62] Istituto dei Sistemi Complessi—CNR and Dipartimento di Energia—Politecnico di Torino, C.so Duca degli Abruzzi 24, 10129 Torino, Italy

[63] Universidad Carlos III de Madrid, Madrid, Spain

[64] Eindhoven University of Technology, Eindhoven, Netherlands

[65] Politecnico di Milano, Milan, Italy

[66] Rudolf Peierls Centre for Theoretical Physics, University of Oxford, Oxford OX1 3PU, United Kingdom of Great Britain and Northern Ireland

[67] Space and Plasma Physics, EECS, KTH, SE-100 44 Stockholm, Sweden

[68] Aix Marseille University, CNRS, IUSTI UMR 7343, F-13013 Marseille, France

[69] EUROfusion Programme Management Unit, Boltzmannstr. 2, 85748 Garching, Germany

[70] University Roma Tre, via Vito Volterra N°62, CAP 00146 Rome, Italy

[71] Lithuanian Energy Institute, Laboratory of Nuclear Installation Safety, Breslaujos Str. 3, LT-44403 Kaunas, Lithuania

[72] V.N. Karazin Kharkiv National University, Kharkiv, Ukraine

[73] Center for Energy Research (CER), University of California-San Diego (UCSD), La Jolla, CA, United States of America

[74] Massachusetts Institute of Technology, Plasma Science and Fusion Center, Cambridge, MA 02139, United States of America

[75] Warsaw University of Technology, Nowowiejska 15/19, 00-665 Warsaw, Poland

[76] Faculty of Mathematics and Natural Sciences, Heinrich Heine University Düsseldorf, 40225 Düsseldorf, Germany

E-mail: Emmanuel.joffrin@cea.fr

CrossMark

Abstract

Within the 9th European Framework programme, since 2021 EUROfusion is operating five tokamaks under the auspices of a single Task Force called 'Tokamak Exploitation'. The goal is to benefit from the complementary capabilities of each machine in a coordinated way and help in developing a scientific output scalable to future largre machines. The programme of this Task Force ensures that ASDEX Upgrade, MAST-U, TCV, WEST and JET (since 2022) work together to achieve the objectives of Missions 1 and 2 of the EUROfusion Roadmap: i) demonstrate plasma scenarios that increase the success margin of ITER and satisfy the requirements of DEMO and, ii) demonstrate an integrated approach that can handle the large power leaving ITER and DEMO plasmas. The Tokamak Exploitation task force has therefore organized experiments on these two missions with the goal to strengthen the physics and operational basis for the ITER baseline scenario and for exploiting the recent plasma exhaust

enhancements in all four devices (PEX: Plasma EXhaust) for exploring the solution for handling heat and particle exhaust in ITER and develop the conceptual solutions for DEMO. The ITER Baseline scenario has been developed in a similar way in ASDEX Upgrade, TCV and JET. Key risks for ITER such as disruptions and run-aways have been also investigated in TCV, ASDEX Upgrade and JET. Experiments have explored successfully different divertor configurations (standard, super-X, snowflakes) in MAST-U and TCV and studied tungsten melting in WEST and ASDEX Upgrade. The input from the smaller devices to JET has also been proven successful to set-up novel control schemes on disruption avoidance and detachment.

Keywords: JET, ASDEX Upgrade, MAST-U, TCV, WEST, Tokamak Exploitation Task Force, EUROfusion

(Some figures may appear in colour only in the online journal)

1. Introduction

The overarching priorities of this EUROfusion tokamak programme are to: (i) prepare ITER exploitation, (ii) guide the DEMO design, and (iii) exploit the recent machine enhancements, in particular those related to plasma exhaust (PEX: Plasma EXhaust). In the new European framework programme (2021–2025), EUROfusion has therefore gathered the experimental tokamak activities under a single structure called Tokamak Exploitation (TE). This Task Force is developing the scientific EUROfusion programme along the European Roadmap using five devices: ASDEX Upgrade (AUG) [1], JET [2], MAST-U [3], TCV [4], and WEST [5]. Taking advantage of the complementary capabilities of each machines, the TE Task Force has developed a unified scientific programme along these three directions in close collaboration with devices domestic programme. In 2021 and 2022, particular emphasize was given to the physics basis of the ITER baseline scenario and strengthening the items for the ITER non-nuclear plasma phases, to the exploration with small or no-ELM (edge localized modes) scenario for DEMO and the investigation of alternative divertor geometries to exploit the new enhancements on AUG [1], MAST-U [3], TCV [4] and WEST [5].

The TE scientific programme has developed strong ties between devices on the operational and physics basis of the ITER baseline scenario. In particular, this has been the case for consolidating the operation of the ITER baseline scenario, the development of disruption avoidance and run-away mitigation as well as plasma breakdown, error field studies and plasma conditioning. Protecting plasma facing components (PFCs) in a fusion reactor requires keeping both steady state and transient heat loads to acceptable limits (typically less than 10 MW/m^2 and <0.5 MJ/m^2 within 0.5 ms for any ELMs [6]) together with ensuring sufficient component lifetimes. In the 2021 and 2022 experimental TE programme, emphasis was therefore given to (i) the investigation of alternative divertor geometries, (ii) the assessment of the ITER relevant tungsten PFCs, (iii) the physics and active control of plasma detachment and (iv) the mitigation of transients (ELMs & disruptions). Taking advantage of the complementary capabilities of each machine, the TE Task Force has developed a unified scientific programme in close collaboration with each device.

This paper is organized along the nine 'research topics' that the TE Task Force has set-up, each addressing a set of specific scientific objectives and using the capabilities of the EU available devices to achieve them:

- *Core-Edge-SOL (scrape-off layer) integrated H-mode scenario compatible with exhaust constraints in support of ITER*. This objective aims at consolidating the operation of the baseline scenario for ITER [7] at low core and pedestal collisionality, and then, develop its compatibility with divertor detachment at high current.

- *Physics understanding of alternatives to Type-I ELM regime*. Extending the parameters space of no- or small ELM scenarios to large Psep/R and/or pedestal top collisionalities is essential preserving the wall integrity in for ITER and DEMO [8]. In addition, the exploration of negative triangularity (NT) is included here since it may lead to the operation of edge-localized mode-free L-mode regime with a larger strike-point radius thus ameliorating divertor power-handling requirements.

- *Strategies for disruption and run-away mitigation*. Disruption and run-away electrons are considered as the first risk for the safe operation of ITER and a fusion power plant [9]. This topic has therefore been given a high priority in the TE programme using SPI (Shattered Pellet Injection) as the mitigation technique with the participation of ITER organization in JET and AUG experiments.

- *Physics-based machine generic systems for an integrated control of plasma discharge*. Developing and testing disruption avoidance and detachment control are two priorities for the future operation of ITER. In addition, this section has also addressed important strategies in support of the ITER scenarios such as the optimization of plasma breakdown, exit and entry to the H-mode and the characterization of error fields.

- *Physics of divertor detachment and its control for ITER and DEMO operation*. The understanding of detachment access is mandatory if detachment control is to be introduced in larger devices like ITER or DEMO [10] as well as finding the optimal extrinsic impurity mix and its extrapolation at higher edge pedestal temperature. This topic is also addressing the physics understanding of edge-SOL particle and heat transport in detached conditions.

- *Preparation of efficient PFCs operation for ITER and DEMO*. High particle and power loads on the ITER divertor require testing actively ITER-grade cooled components up to the maximum particle fluence [11]. This research topic also addresses fuel retention and removal (with relevant conditioning methods) and the quantification of material erosion from metallic wall under plasma conditions relevant for ITER.
- Physics understanding of alternative divertor configurations as risk mitigation for DEMO. Alternative divertor configurations have recently emerged in response to the DEMO divertor target requirements. This topic exploits in particular the new PEX upgrade in MAST-U and TCV and quantifies the ELM heat loads and detachment conditions in those configurations. PEX upgrades on AUG will be available by the end of 2024.
- *Physics and operational basis for high beta long pulse scenarios*. A viable solution for a stable steady state scenario at high β remains an important objective for the TE Task Force in view of JT-60SA and DEMO. This part aims also at defining the required control schemes and, in the more long term, the compatibility of long high β pulses with the wall constraints [12].
- *Physics understanding of energetics particles confinement and their interplay with thermal plasma*. This research topic focusses on understanding and quantifying the stabilization of ion core turbulence by energetic particles and fast ion losses by MHD instabilities with the ultimate goal improving the prediction of burning plasmas performance.

The results below are summarizing the main results of the task force since 2021. They demonstrate the importance of combining the input of several devices to achieve the scientific objectives of each research topic.

2. Core-Edge-SOL integrated H-mode scenario compatible with exhaust constraints in support of ITER

2.1. Strengthening the physics basis of the ITER baseline scenario

The ITER baseline scenario (IBL) has been jointly investigated on AUG [13, 14] and TCV [15, 16]. The recent developments in TCV were made possible with the installation of an NBI heating source, allowing ELMy H-modes at ITER relevant $\beta_{\rm N}$. The IBL scenario is mainly characterized by low q_{95} (3.0–3.6), high positive triangularity (PT) ($\delta > 0.35$) and relatively high elongation ($K > 1.65$) and normalized beta ($\beta_{\rm N} > 1.5$). In AUG, these combinations lead to very steep and narrow edge transport barriers, when good confinement is obtained, with high pedestal pressure and therefore large type-I ELM crashes. A similar behaviour is also observed on TCV where discharges with similar confinement properties ($H_{98} \sim 1$) and normalized beta ($\beta_{\rm N} \sim 1.8$), as those expected for the ITER baseline scenario, have been obtained. TCV IBL performance is mainly limited by (neoclassical) tearing modes, in particular 2/1 modes. They can be avoided with
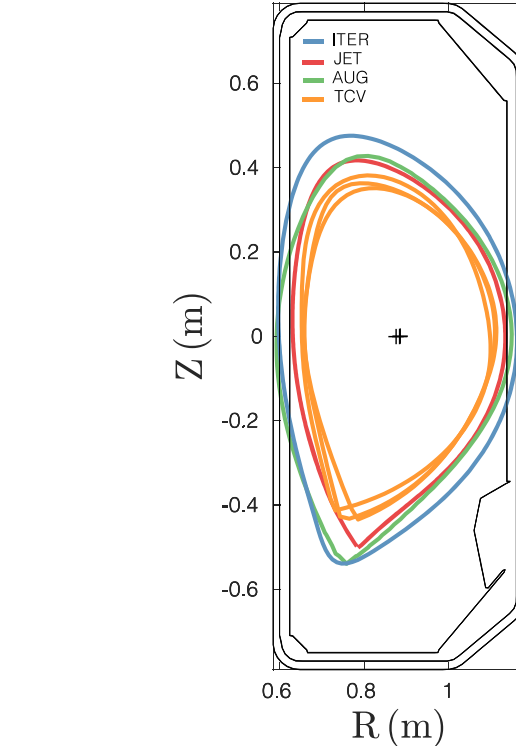

Figure 1. ITER Baseline plasma shapes developed at TCV (orange) to AUG (green), JET (red) and ITER (blue). The aspect ratio is kept constant. Reproduced from [16]. © The Author(s). Published by IOP Publishing Ltd. CC BY 4.0.

central X3 EC heating at relatively high q_{95} and moderate $\beta_{\rm N}$. However, the lack of significant ECH at the high central densities obtained in the TCV IBL scenario limits the duration of low q_{95} cases to about six confinement times. During this time, the current density can fully evolve and the density usually keeps peaking until (neoclassical) tearing modes are triggered (N)TM. Integrated modelling results show that ion temperature gradient (ITG) modes are the dominant instabilities in both AUG and TCV IBLs and that, in TCV, NBI fuelling also plays a role to sustain the mainly turbulent-driven significant peaked density profiles.

In TCV, type-I ELMs are also challenging for achieving a stable ramp-up in TCV, as the large ELMs challenge vertical stability and frequently trigger NTMs. It is shown in TCV that the issue is alleviated, when entering into H-mode at reduced top triangularity, as the ELMs are more frequent under these conditions. The triangularity is then subsequently increased during the H-mode phase. This strategy helps avoiding large early ELMs entering H-mode and can be applied in ITER. Entering H-mode at higher q_{95} is also efficient to avoid the NTMs seeded by ELM crashes. Using this strategy, IBL shapes investigated at AUG (and at JET in past experiments), but also the foreseen ITER shape have been reproduced at TCV (figure 1). Similar to the shaping technique, $I_{\rm p}$ can then be increased once in H-mode, which is also a strategy applicable in ITER. Like in TCV, recent studies at AUG have shown that the stability of the plasma is strongly improved when entering a small ELM regime at low heating powers and

large D2 fuelling gas puff. Safe termination has been demonstrated at $q_{95} \sim 3$ on AUG and $q_{95} \sim 4$ at TCV [16] utilizing predictive optimization using the RAPTOR code. The main ingredients for a safe and yet rapid termination are a decrease of plasma current together with a decrease of elongation, while controlling the heat sources during the whole termination to control the power balance as also done in JET [17]. The goal being to trigger an H-L transition at about 1/3 of the ramp-down, the elongation should not decrease too fast, to avoid too low q_{95} values and the H-L transition should not occur too late to avoid a too large Greenwald fraction. These key ingredients allow a control of the time evolution of the internal inductance, elongation and power balance. These studies have also been used to develop the real-time termination algorithm used in JET baseline scenarios.

In summary, the ITER baseline scenario has been developed in AUG and TCV with good performance using the same plasma shape than JET and in the future ITER. The stability domain at function of q_{95} and β has been identified and the H-mode exit strategy optimized using RAPTOR simulations.

2.2. Towards the development of radiative scenario at low collisionality

Based on these results, partial detachment requirements for the ITER baseline scenario have then been tested in TCV using nitrogen seeding but resulted in larger ELMs [16]. In ASDEX Upgrade, the parameter space of the ITER baseline H-mode with reduced ELMs has also been explored via impurity seeding of Ar and Kr with varying heating power. In particular, this helped to achieve the regime with larger heating powers. In both devices, more experiments are needed to develop the radiative scenario [14].

In JET, an integrated, Ne-seeded H-mode at 2.7 T/2.5 MA was first demonstrated in previous campaigns at high power [18]. This scenario is using an ITER-like shape as shown on figure 1 (similar to the TCV and AUG shapes) with an upper triangularity of $\sim$0.35 and the strike points on the vertical divertor target. Note that this JET scenario is different from the baseline scenario developed for the DTE2 campaign (upper triangularity of 0.2 and strike points in the divertor corner) to maximize the fusion power [19] without impurity seeding. The JET Ne-seeded scenario could be achieved in stationary conditions for 5 s with about 30 MW of input power, $H_{98(y,2)} = 0.9$, $\beta_N = 2.2$, and a radiative fraction of 86% with very small ELMs (less than 0.3% variation in stored energy), strongly reduced divertor temperature and partial detachment. It was shown recently that the level of confinement in Ne-seeded discharges was likely achieved thanks to the higher pedestal temperature and increased angular rotation [20]. This scenario was then adapted and run for the first time in a 50–50 D-T mixture in JET with the ITER-like wall at 2.5 MA during DTE2 campaign [18].

Building on this previous successful JET neon seeded radiative scenario and on the results in AUG and TCV presented above, the more recent programme of the TE task force is extending the operational space at higher plasma current (up

to 3.2 MA/3.45 T) towards lower core and pedestal collisionality with partial detachment and documented both N$_2$- and Ne-seeded scenarios for comparison with modelling in view of the extrapolation to ITER [21].

3. Physics understanding of alternatives to Type-I ELM regime

In reactor scenarios, strict conditions will be imposed on transient heat loads resulting from ELMs that are a common feature of the ITER baseline scenario. The quasi-continuous exhaust (QCE) scenario developed on AUG and then exported to TCV is an attractive ELM-free regime (showing a broadening of the SOL power fall-off length and a low concentration of high-Z impurities in the core). A physics picture explaining this regime starts to emerge: ballooning modes near the last closed flux surface governed by the pressure gradient and the magnetic shear are destabilised through various effects [22–24].

In TCV, the impact of plasma shaping on the properties of SOL profiles and transport at the outer mid-plane has been investigated through a dedicated database of TCV discharges ranging from type-I (low δ) to QCE (large δ). Both parallel heat load and near-SOL density profile broaden significantly at increasing α_t, whereas in the far SOL a density shoulder has been observed to form when moving from low to high δ_u. An enhancement of radial turbulent particle transport is observed [25]. In ASDEX Upgrade, the operational space with respect to the separatrix conditions, the so called 'SepOS' [26], is established for QCE and compared to type-I ELMy plasmas [27] (figure 2). Significant broadening of the power fall-off length is observed, correlating to an increased separatrix density and pressure. Both TCV and AUG exhibit flatter SOL density profiles at higher values of α_t, where theory predicts the plasma to be more resistive interchange unstable. The flattening of density profiles is accompanied as well by an increase of the heat flux decay length and an increase of the fraction of energy towards the first wall [28]. An observed increase of fluctuations in the near and far SOL in the high turbulence regime is suggestive of an increase of convective filamentary transport as primary cause of increased energy and particle load towards first wall. The reactor relevance of the scenario was demonstrated by expanding the operational space to low edge safety factor and demonstrating the benign tungsten impurity behaviour [27].

This no-ELM regime has been exported to JET to gain more confidence in the scenario by demonstrating it in a larger device. The QCE scenario has been successfully developed at JET building on knowledge gained from previous experiments in ASDEX Upgrade and TCV, namely high plasma shaping and high density/pressure at the vicinity of the separatrix through strong gas puffing [29].

In the last years, the Enhanced D-Alpha (EDA) regime, which has similarities to the QCE, has also gained maturity on AUG [30]. Various parameter scans showed that increasing heating power raises core and edge temperature, while higher gas puff leads to a small density increase and extends the
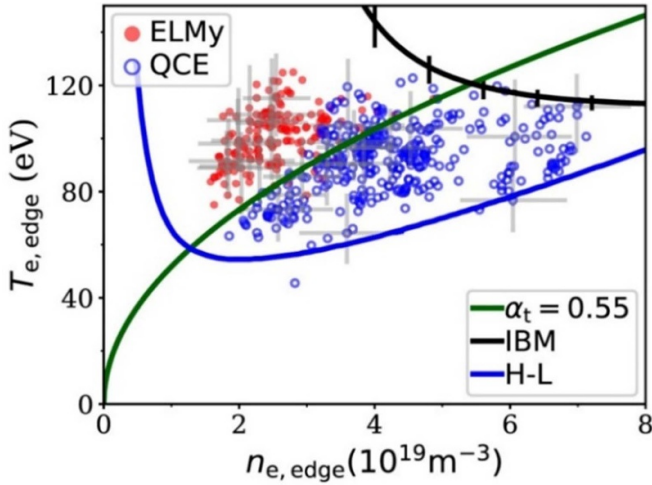
Figure 2. AUG separatrix operational space in edge density $n_{e,edge}$ and temperature $T_{e,edge}$ of the data set with $B_T = -2.5$ T and $I_p = 0.8$ MA. Open blue symbols represent QCE phases, filled red symbols represent type-I ELMy phases. Reproduced from [27]. © 2023 The Author(s). Published by IOP Publishing Ltd on behalf of the IAEA. All rights reserved.

no-ELM power window. Impurity seeding in EDA H-modes resulted in some of the best core-edge integration solutions among no-ELM regimes. Stationary discharges with nitrogen seeding proved very effective in increasing radiation and lowering divertor temperature while maintaining good energy confinement, as well as the presence of the Quasi-Coherent Modes (QCM) and no ELMs. Argon seeding allowed for pedestal radiative cooling, not only reducing the power flowing to the SOL, but also extends the no-ELM power window. An experimental characterisation of the QCM and its impact on the pedestal transport was found to be challenging and more dedicated experiments seem necessary. Similarly, to the QCE regime, the EDA regime has been established on JET in the recent months. Interpretation with modelling has also progressed in particular with non-linear extended MHD simulations with JOREK showing partial agreement with the experimental observations [31].

L-mode plasmas with NT are another example of natural ELM-free regime. Indeed, a necessary condition for the access to H-mode is the accessibility of 2nd ballooning stability near the edge, which is avoided with sufficiently NT at either the top or the X-point (taking a lower-single-null shape as) [32]. Recent experiments have been carried out on TCV and AUG using the PT and NT shapes in similar ITG dominant transport conditions. They have shown an encouraging picture regarding NT effects. In TCV, a strong beneficial effect of NT that allows NT L-modes to largely overcome the performance of corresponding PT plasmas is shown, reaching the central pressure and temperature values of higher power H-modes. AUG also shows cases where NT plasmas reach central values comparable to PT plasmas. The beneficial effect of NT was confirmed by gyrokinetic runs to be due to an increase of the critical temperature logarithmic gradient when inverting the triangularity, with similar stiffness for positive and NT. The

effect has been found in both ITG- and TEM-dominant micro-instability regimes [33]. In both tokamaks, part of the better performance of NT seems to be coming from the SOL, resulting in larger *n, T* at the last closed flux surface. In TCV, it was also noted that the measured temperature peak at the outer strike point is higher in NT than in PT [34]. Indeed, experiments and simulations points towards lower λ_q in NT configuration L-Mode compared to the PT L-Mode. Power exhaust may remain a challenging question for NT in future experiments.

In the past 2 years, ELM-free regimes established in AUG have been successfully exported to TCV and is now attempted in JET to gain confidence on its operation in a larger device. In addition, NT discharges in TCV and AUG have demonstrated better performance than PT pulses possibly coming from the different edge conditions. These are important progress towards the design of ITER and DEMO scenarios with reduced heat loads to the wall.

4. Strategies for disruption and run-away mitigation

4.1. Disruption mitigation studies with shattered pellet injection

The integrity of ITER's PFCs can also be put at risk by thermal and magnetic energy losses during the thermal and current quench (TQ & CQ) phases of disruptions and/or impacts of high-energy runaway electrons. In JET, an upgraded shattered pellet injector (SPI) system was tested to enhance pellet assimilation to obtain the higher radiative fraction (>90%) required for ITER (figure 3). Following the recent installation [35] and experiments [36] with the SPI on AUG, the use in JET [37] provides an up-scaling approach for ITER for the mitigation of heat loads at the TQ and CQ. Recently JET has been able to investigate single, staggered and dual pellet injection with different Ne/D ratio showing different levels of particle assimilation [38]. In addition, the JET Thomson scattering diagnostic has been modified to measure the density evolution at the time the pellet penetrates the plasma. These data are essential for constraining the JOREK modelling [39] in view of the predictions to ITER.

Using the upgraded SPI, JET has for example validated its use for the mitigation of vertical displacement event (VDE) in ITER, which can cause deleterious electro-magnetic (EM) loads on the vessel of tokamak and thermal loads on the PFCs. It is found that SPI can prevent the toroidal asymmetrical phase of the VDE, i.e. AVDE and the exponential growth of the plasma current centroid vertical position is interrupted and stabilised (figure 4). In addition, it was demonstrated that the vessel reaction forces are strongly reduced in mitigated VDEs and was demonstrated that the difference in the energy deposited to the beryllium upper dump plates is about 5 times less than for unmitigated VDEs. From these results, it can be concluded that the SPI can be considered as a reliable method for protecting a machine from VDE although more modelling and experiments would be needed to extrapolate these results to ITER [40, 41].
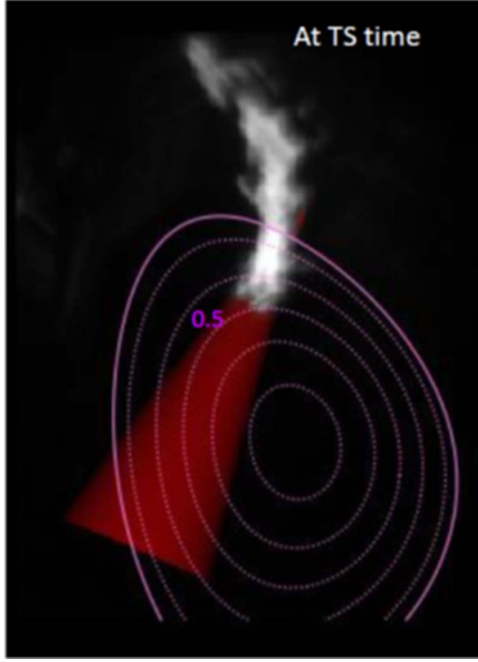
Figure 3. H$_\alpha$ cloud recorded by the JET fast camera at the time of the pellet penetration. The overlaid equilibrium is the last prior to the pellet arrival. Reproduced with permission from [38].
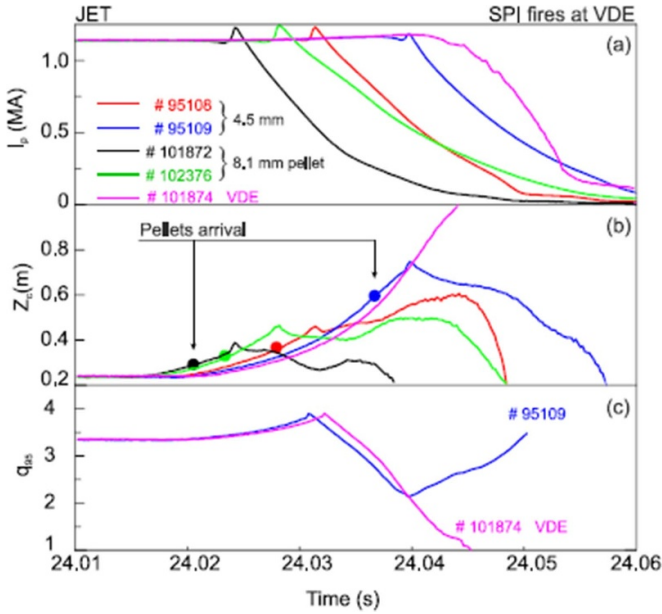

Figure 4. Suppression of VDE by SPI (*a*) plasma current, (*b*) current centroid vertical position, (*c*) q_{95}. Reproduced with permission from [41].

4.2. Run-away mitigation

A benign termination technique for run-away electrons (RE) has been developed in both AUG and TCV, and their operational space explored in a systematic manner. It was found that benign termination requires a low density companion plasma, which is achieved through cooling via neutral conduction. An upper limit in neutral pressure was observed and attributed to increasing collisions between the REs and neutrals, leading to a rise in the density of the companion plasma. Complete expulsion of run-away and conversion of magnetic energy to radiated energy was observed at the final collapse. The efficacy of this conversion was linked to the MHD mode growth rate and neutral pressure at the time of collapse. This technique was successfully used at run-away currents of up to 600 kA on ASDEX Upgrade with maximum heat fluxes to the wall below what is observed in a non-benign termination at 200 kA [42, 43].

More recently, JET has continued to developed run-away mitigation by injecting a large amount of low-Z species (hydrogen or deuterium) with the SPI [44]. It is found that the ability of the deuterium or hydrogen to lead to benign termination is a complex interplay between the amount of impurities still present in the cold companion plasma, the vessel neutral pressure, the runaway current and the injection timing with respect to the natural evolution of the beam. Limits of this scheme are being explored and as well as the characterization of the companion plasma in benign vs. non-benign situation [45].

Disruption mitigation has been explored intensively with the JET SPI and further experiments are planned in AUG with an SPI injector with different capabilities (i.e. different shattering angles) than the JET one. In JET, mitigation of VDEs with the SPI has been demonstrated experimentally and is reproduced via modelling. In addition, mitigation of run-away electrons using pure deuterium or hydrogen gas injection has been demonstrated in AUG and TCV and the limits of these schemes characterized with respect to the companion plasma and vessel neutral pressure.

5. Physics-based machine generic systems for an integrated control of plasma discharge

5.1. Disruption avoidance

Disruption avoidance is a major topic that the TE task force has addressed in the past 2 years in AUG and TCV. Efforts have been made to reproduce control networks on several devices for a specific disruption avoidance type as well as optimized error field identification and plasma breakdown for ITER (see the next two sections as well). Within the EUROfusion programme the disruptive H-Mode density limit (HDL) has been studied further on three devices (ASDEX Upgrade, TCV and JET) [46]. Advanced real time control coupled with improved real time diagnostics has enabled the routine disruption avoidance due to the HDL. This allowed the systematic study of the influence of various plasma parameters on the onset and behaviour of the HDL in regimes not easily accessible otherwise. The upper triangularity δ_{top} of the plasma is found to have a significant influence on the X-Point Radiator (XPR, see section 6 below), which plays a major role for the evolution of the disruptive HDL [46]. At high δ_{top} the gas flow at which the onset of the XPR occurs is strongly reduced compared to low triangularity. The reduction of the upper
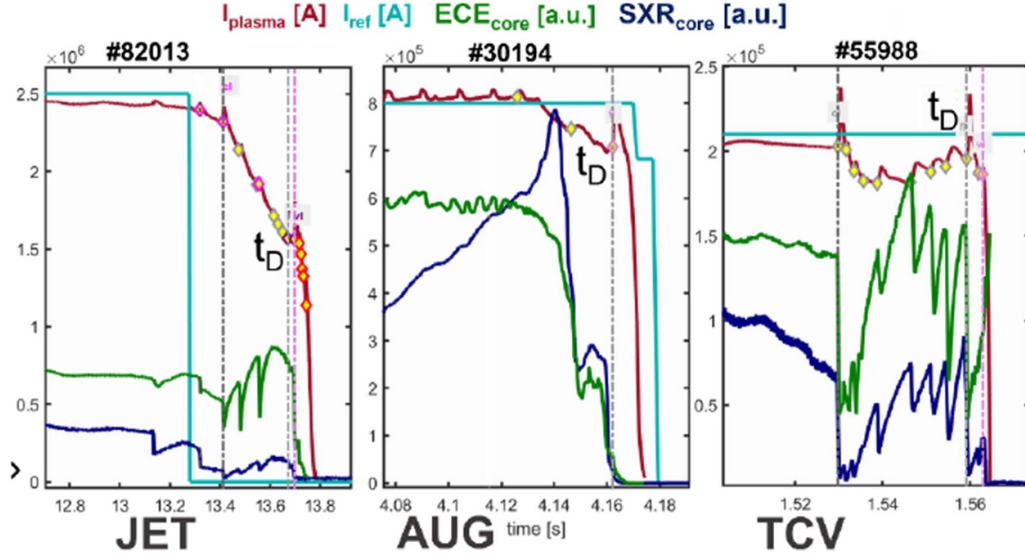
Figure 5. Automatic calculation of disruption characteristic times based on the correlation of various quantities, where I_{plasma} is the actual plasma current, I_{ref} is the reference plasma current, ECE_{core} and SXR_{core} are proxies for the core temperature based respectively on Electron Cyclotron Emission and on Soft x-rays diagnostic. Reproduced with permission from [48].

triangularity δ_{top} has proven to be an effective actuator for the HDL disruption avoidance on ASDEX Upgrade. The stable existence of the XPR, which is thought to be a requirement for detachment control in future devices, influences the behaviour of the HDL. This control scheme of a simultaneous feedback control of empirical disruptive boundary and edge density was imported from AUG to TCV and successfully tested [47]. The avoidance of disruptions due to density limits has been integrated and tested in real-time, demonstrating the capability of recovering the H-mode scenario after the H-L back transition and the strong degradation caused by the onset of a MARFE instability, i.e.; the XPR moving upwards. This test case control has been exported to JET and implemented to demonstrate its applicability on a larger device [46].

In addition, a novel concept has emerged for the construction of a standardized multi-machine disruption database and the detailed study of JET disruption characteristics over the last 10 years. The EUROfusion Disruption Database (DDB) includes a fully automated workflow to build and validate a multi-machine database based on standardized definition of characteristic disruption parameters, such as thermal quench (TQ) time, current quench (CQ) time, minor and major disruption times (t_D), VDE, runaway electrons (RE) phases, etc (figure 5) [48]. Moreover, it integrates various tools to ensure reproducibility, data provenance tracking (data & code version control based on continuous integration/deployment tools), and compatibility with the ITER Integrated Modelling & Analysis Suite (IMAS) framework [49]. Thanks to these features, the framework developed is machine-generic and can be easily transferred to any other machine, including ITER for supporting empirical scaling or modelling activities and enabling the development of Machine Learning (ML) and Artificial Intelligence (AI) technologies for disruption prevention.
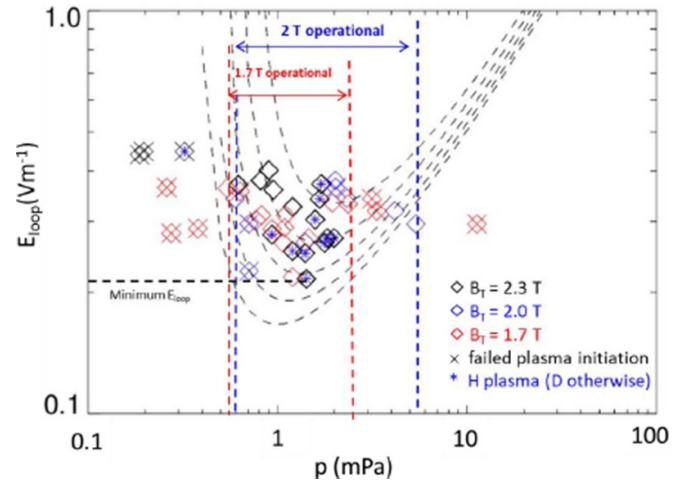

Figure 6. Toroidal (loop) electric field versus prefill gas pressure, both at the time of breakdown, for all attempted IC assisted breakdown discharges in this study with $B_T = 1.7$ T (red squares), $B_T = 2.0$ T (blue squares), and $B_T = 2.3$ T (black squares). Reproduced from [50]. © The Author(s). Published by IOP Publishing Ltd. CC BY 4.0.

5.2. Plasma breakdown in ITER conditions

For the first time in JET, both ion cyclotron (IC) assisted and Ohmic breakdown were achieved in D for the regime planned for the first pre-fusion operation (PFPO-1) phase of ITER, $E_{loop} \lesssim 0.33$ V/m with $B_T = 1.7$ T and where Electron cyclotron (EC) breakdown assistance with 170 GHz waves would not work. Plasma initiation with IC assisted breakdown was significantly more robust than Ohmic breakdowns with the same toroidal electric field and B_T [50] (figure 6). Similar encouraging experiments are underway on WEST with a full tungsten wall.

On ASDEX Upgrade, a series of dedicated experiments have been performed using EC heating (X2) with a controlled Ne impurity injection in the prefill phase, to mimic non-favourable burn-through conditions such as those expected in a discharge following a disruption event. These experiments showed that optimised settings of ECH power (onset and duration of the pulse) have played a key role in allowing the early Ne burn-through (with Ne concentration up to 14% and EC power of 1.4 MW) [51]. Recent experiments with low breakdown loop voltage on WEST have also been carried out and will be continued in 2024 in a full tungsten wall. For an efficient and robust use of such a technique, it is essential to develop appropriate models capable of describing present experiments and of extrapolating to (or predicting) future scenarios. A novel, model-based, automatic method to obtain the desired magnetic field evolution during the breakdown and early (feedforward) ramp-up phase, proposed for use on JT60-SA and ITER, has been successfully tested for the first time on TCV [52].

5.3. Error fields detections

Error Fields (EFs) are non-axisymmetric fields present in tokamaks [53], which can potentially drive a plasma disruption [54]. During ITER operation, the number of allowed disruptions is very limited, especially when exploring high plasma current regimes ($I_p > 5$ MA) [55]. A careful detection of EF sources and their correction is thus crucial for a successful operation of ITER, including the design and test of robust and reliable disruption-free methods for EF identification. To detect EFs, the compass scan method has been routinely deployed on tokamaks worldwide and relies on the locked mode (LM) onset [56] and was recently used in MAST-U [57]. However, the LM induced can have a potentially disruptive behaviour. To encompass this issue, recently a non-disruptive compass scan method has been tested in the DIII-D tokamak ohmic plasma scenario [58]. Similar to the conventional compass scan, an increasing probing field is applied until a LM forms. When the LM detector detects this event, the plasma controller engages asynchronous density and EFCC control waveforms that enable prompt healing of the magnetic island. To assess the portability of the non-disruptive compass scan method to ITER, experiments have been performed within Work Package Tokamak Exploitation at JET and in MAST-U ohmic plasma scenarios [59]. Promising results have been obtained, which demonstrate the high fidelity of the method. In particular, in JET the magnetic island healing has been achieved not only by gas puff, as in DIII-D, but also with pellet injection. This paves the way of using pellets to increase the density in ITER during the non-disruptive compass scan method, which is the preferable actuator because of the slow time response of the gas valves (hundreds of ms with gas vs tens of ms with pellets) and better particle penetration of pellets. The first EFCC/density asynchronous controller design for ITER-PFPO-1 based on these experimental results is described in [59].

The three sections above illustrate the progress done in controlling plasma discharge: similar disruption avoidance

control schemes have been developed on two devices (AUG and TCV), RF-assisted plasma breakdown have been demonstrated at electric fields close to those expected for plasma breakdown in ITER and a new method for error field detection tested successfully. These results are important for consolidating the operation of the future ITER plasma discharges.

6. Physics of divertor detachment and its control for ITER and DEMO operation

Separately from the development of the radiative scenario (see section 2.2), this section addresses the detachment physics and control studies achieved by the TE programme in the past 2 years. Controlling plasma steady state heat loads is indeed key topic for ITER and efforts to develop sophisticated controllers have been undertaken. For this, the X-point radiation (XPR) [62] has become an attractive exhaust solution, featuring full detachment at a radiated power fraction of 90% and a moderate confinement reduction. An XPR scenario is now established at AUG [62], TCV [60], WEST [5] and JET. Plasma detachment is typically induced by impurity seeding during the heating phase. In AUG, for the first time full detachment with a 90% radiation fraction across the whole discharge (including the transitions in and out of H-mode) was achieved by employing X-point radiation (XPR) [61] (figure 7). The XPR is monitored in real-time and regulated by nitrogen injection. The parameter space for operation with the XPR was significantly extended, using this active feedback. The XPR (location) acts as a buffer for the fast changing power flux during the LH transition, which allows controlling actively and ensuring the detached state. The XPR can now routinely be established in SOLPS simulations for AUG [63] and TCV [64]. The ELM suppression, connected to a high location of the XPR above the X-point, is also observed in the whole parameter range. Direct measurements of density and temperature from the XPR region using the new divertor Thomson scattering system at AUG indicate that a cold XPR core is developing behind a radiating shell. Whether this cold XPR core exists as soon as the radiator develops cannot be concluded yet. An XPR is also observed in TCV by the injection of nitrogen as extrinsic impurity. This highlights that the wall material (W for AUG, C for TCV) or machine size does not play a significant role for the existence of the regime. However, the scenario appears to be less stable for TCV. First experiments show the necessity of an active control for this scheme as demonstrated in AUG: the required nitrogen seeding level changes can lead to a radiative collapse of the plasma, if the wall conditions and the wall storage of nitrogen change.

Also, in a recent study on AUG, it was demonstrated that divertor reattachment from weakly detached conditions was primarily set by the core energy confinement time, while reattachment from strongly detached conditions incurred an additional delay primarily governed by the energy needed for re-ionization of the divertor neutral particles [65]. The work has been extended as well to larger devices, namely JET, revealing that the time required for full re-ionisation of the neutral volume between the X-point and outer divertor target under
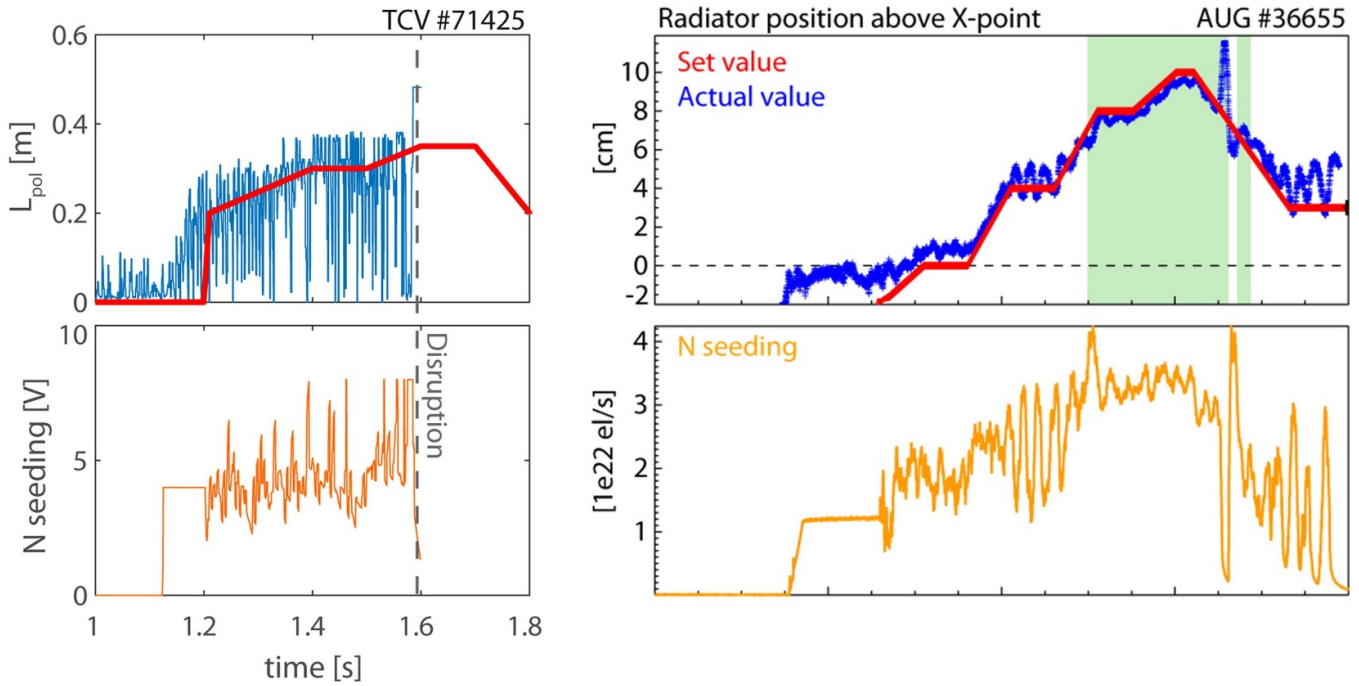
Figure 7. Position control of the XPR by nitrogen injection in TCV (left) and ASDEX Upgrade (right). The X-point radiator exists independently of the wall material or device size. Reproduced from [60]. CC BY 4.0. Reproduced from [61] © 2024 The Author(s). Published by IOP Publishing Ltd on behalf of the IAEA and EURATOM. All rights reserved.

fully detached conditions is approximately 1 s on JET [66]. Significant progress was achieved understanding the mitigation of the heat-flux deposition during ELMs on AUG in radiative scenarios. Plasmas with extrinsic seeded impurities have been performed on AUG, where it has been highlighted that Ar seeding is necessary to achieve significant buffering of ELM energy ($f_{buff} > 40\%$) [67].

The successful XPR control achieved throughout both the L-mode and H-mode phases in AUG and the complementary results in TCV and WEST demonstrate that the control of steady state heat load can be established independently from the device. Similar exploration presently done in JET will pave the way towards the design of a core-edge integrated scenario in ITER.

7. Preparation of efficient PFCs operation for ITER and DEMO

7.1. Advances in the qualification of ITER grade components

The installation of the full tungsten ITER grade actively cooled components was completed in WEST in 2021 within the PEX Upgrade [68] and was followed by the first high fluence campaign, using repetitive long pulses to accumulate ITER relevant fluence on the divertor [5, 69]. Actively cooled, tungsten components with exposed poloidal gaps showed crack-network patterns. The present understanding is that this is due to the impact of transient heat loads (such as disruptions) on cold mono-blocks [70, 71].

An experiment has been carried out in AUG to examine the power loading from ELM ions penetrating in toroidal gaps.

ELM-expelled ions can indeed penetrate gaps established between individual mono-blocks in the toroidal direction and induce large heat loads on the monoblock structures, especially close to the entrance into the gap. This phenomenon was studied on AUG using H-mode discharges with large type-I ELMs, both in the standard and reversed B_T/I_p configuration, with the help of thin Pt-coated marker gap samples implemented on the AUG divertor manipulator. The experimental results agree with ion-orbit simulations and indicate strong penetration of the ions into the gaps, resulting in erosion of the Pt markers at depths down to ~1 mm [72]. In addition, reversing the field and current directions also results in reversal of the erosion patterns between upper and lower side faces of the gap (in the poloidal direction). It is worth noticing that the erosion patterns cannot be explained solely by considering guiding centre motion along magnetic field lines but the direction of the ion orbits (field & current reversal) has to be taken into account. In WEST, hot spots, which were predicted to happen in ITER at toroidal gap crossings [70], were evidenced experimentally through post exposure examination of the divertor Plasma Facing Units (PFU) [73]. A first experiment was carried out using the Very High Resolution Infra-Red camera of WEST to measure associated heat loads during operation. Analysis has shown that the interpretation of infra-red data in the gap areas requires extensive modelling using photon ray tracing codes, as in addition to usual reflection issues with metallic PFU, gaps are prone to a 'cavity effect' amplifying the infra-red signal [74, 75]. Experiments at higher power are needed to have a clear evidence of the gap heat loading. Concerning W melting, experiments have been carried out on AUG to investigate bridging of tungsten
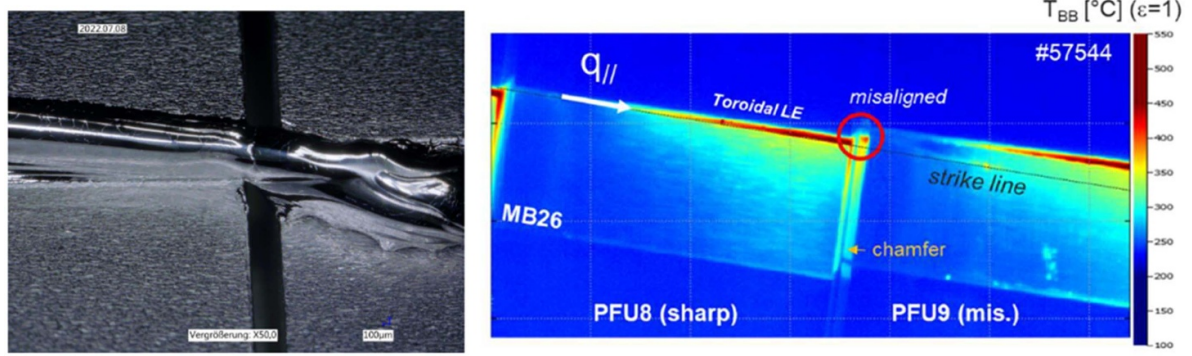
Figure 8. Left: Zoomed-in final deformation profile near the gap in ASDEX Upgrade. Reproduced from [76] © 2024 The Author(s). Published by IOP Publishing Ltd on behalf of the IAEA. All rights reserved Right: infrared image of the plasma-facing unit with 1.5 mm misalignment in WEST. Reprinted from [74], Copyright (2023), with permission from Elsevier.

mono-block gaps by moving melt fronts and resulting from successive melt events caused by transients [72]. The experimental findings of the bridging event (figure 8) were validated by MEMENTO simulations and indicate that the melt will relatively freely cross the gaps without penetrating into the gap [76]. On the other hand, melting experiments by steady state heat loads on actively cooled tungsten components have been carried out in WEST, using a dedicated PFU with a machined groove to expose the subsequent PFU leading edge (figure 8). This has allowed to benchmarking the MEMENTO code under a regime of shallow melting/slow melt layer motion obtained under such conditions for actively cooled components [73].

7.2. Erosion and retention studies in metallic wall

Erosion of Tungsten (in JET, AUG, WEST) and Beryllium (in JET) is comprehensively investigated in EU metallic tokamaks. As in AUG and JET, strong erosion and deposition patterns have been observed on the High Field Side of all machines, most strongly in the divertor region after the first phase of WEST operation. Although the result of different plasma conditions in WEST (L-mode) and AUG (ELMy H-mode), the W net erosion at the outer strike point is estimated in the range of 0.1 nm s^{-1} in attached plasmas for both cases [68].

JET experiments recently identified the role of Beryllium chemically assisted physical sputtering (CAPS) of inner wall limiters with extensive modelling of the intra- and inter-ELM tungsten erosion (with ERO2.0). The role of chemically assisted physical sputtering of Be was investigated by carrying out a series of limiter pulses: by heating the limiter up to clarify the temperature dependence of sputtering. This was done both with and without Ne and N_2 seeding. The measured sputtering yield of Be shows a clear dependence on surface temperature such that the CAPS component vanishes at higher temperatures. This is proposed to be due to the formation of BeD_x molecules. In a new set of experiments, the role of enhanced impurity concentration in sputtering could be distinguished from that of the surface temperature. Especially, the Ne data shows that medium-Z seeding is not the driver for the observed erosion patterns but a strong chemical dependence

is apparent. Quite surprisingly, also in helium plasmas CAPS was observed together with a noticeable BeH signal. This suggests that hydrogen (or deuterium) from previous discharges is persistently retained in the wall (or deposits on top) and can contribute to the erosion even after extended periods in helium [77–79]. W erosion, both in the inter- and intra-ELM phases, has also been investigated on JET and WEST and extensively modelled using ERO2.0. Focus has been put on understanding the role of CX ions on main-chamber erosion, which has been observed to be noticeable. In WEST, first 3D simulations have been carried out, outlining the importance of adequately modelling discrete limiters to assess the global tungsten erosion source.

Fuel retention has also been investigated on JET both with the help of gas-balance experiments and using the newly installed Laser-Induced Desorption Quadruple Mass Spectrometry (LID-QMS) diagnostics [80]. In the gas-balance experiments the amount of injected gas retained in the vessel during a series of identical plasma discharges has been determined. So far the results have been inconclusive, however, detailed analyses are ongoing and their outcome will be reported elsewhere. LID-QMS, for its part, has recently been commissioned and used to clean wall tiles at the inner divertor of JET as well as monitor accumulation of fuel (including T) on them during subsequent plasma operations.

7.3. Wall conditioning

Wall conditioning and fuel control methods in PFCs have been optimized in several EU devices using high power ion and electron cyclotron (IC & EC) injection to control the release of impurities from the first wall and affect recycling of hydrogenic fuel fluxes (H, D, T). This is used to constrain the predictions of the efficiency of IC & EC conditioning in view of the initial phase of ITER [81]. Experiments on ECWC have been carried out on AUG and TCV. On AUG, particular focus points were scanning the location of the resonance layer as well as the vertical B field, with the goal in optimizing the uniformity of the discharges. On TCV, similar scans were performed, partly as a continuation of earlier works [82]. The main outcomes of this exercise were that the vertical field has a strong role

in improving the confinement, stronger than ECWC absorption. Scanning the field can also improve reaching different main-chamber areas and thus condition them, however, on AUG, reaching the high-field side regions remain a challenge. Modelling of the results using the TOMATOR code is ongoing [83].

In addition, changeover experiments have also been executed on JET and WEST. For JET, this was done in connection with the He campaign [84, 85], by investigating the fuel retention characteristics in connection with He $\rightarrow$ H and H $\rightarrow$ He transitions, both when applying ICWC and regular plasma pulses in tokamaks. The JET results show that in a metallic device (with Be and/or W) the changeover down to residual gas levels of 2%–5% can be accomplished with ~10-15 ICWC pulses and ~5 plasma pulses and that the H $\rightarrow$ He transition is clearly faster [86]. On WEST with a full tungsten wall, D $\rightarrow$ H and H $\rightarrow$ D transitions were investigated. These were observed to take more time than anticipated to reach the desired isotopic saturation level. This is thought to be due to strong recycling of the H or D particles thus slowing down their exhaust from the vessel.

The previous three sections illustrated the progress made on plasma wall interaction using EUROfusion metallic devices AUG, WEST and JET: the toroidal gap heat loading has been understood and can now be predicted for ITER components, the first in-situ fuel retention diagnostic (LID-QMS) has been commissioned successfully in JET and RF (IC or EC) wall conditioning has been optimized and successfully used for both conditioning and fuel recovery in several devices. These advances are increasing confidence in future plasma operation in a full metallic wall environment and improving the understanding on erosion of plasma-facing components in various plasmas, including T and He.

8. Physics understanding of alternative divertor configurations as risk mitigation for DEMO

Using the recent PEX (Plasma EXhaust) upgrades, both MAST-U and TCV have developed long leg divertor geometries (figure 9) demonstrating increased capabilities in mitigating heat fluxes both in L- and H-mode discharges. Increasing divertor leg length facilitates access to detachment and provides a wider detachment window, proportional to the leg length L_{leg}. This is mostly attributed to an increased level of divertor volumetric power dissipation with increasing L_{leg}, rather than a SOL width increase [87]. Modelling using SOLPS-ITER confirms that tightly baffled, long-legged divertor performance is mainly due to a better neutral confinement with improved plasma-neutral interactions in the divertor region [64]. In MAST-U, studies of plasma exhaust have concentrated on comparing conventional and Super-X divertor configurations [88]. In L-mode discharges, the separatrix density required to detach the outer divertors is approximately a factor 2 lower in the Super-X than the conventional configuration, in good agreement with SOLPS-ITER simulations [89]. The importance of increased divertor volume in extended outer leg divertor configurations has been studied in intermediate
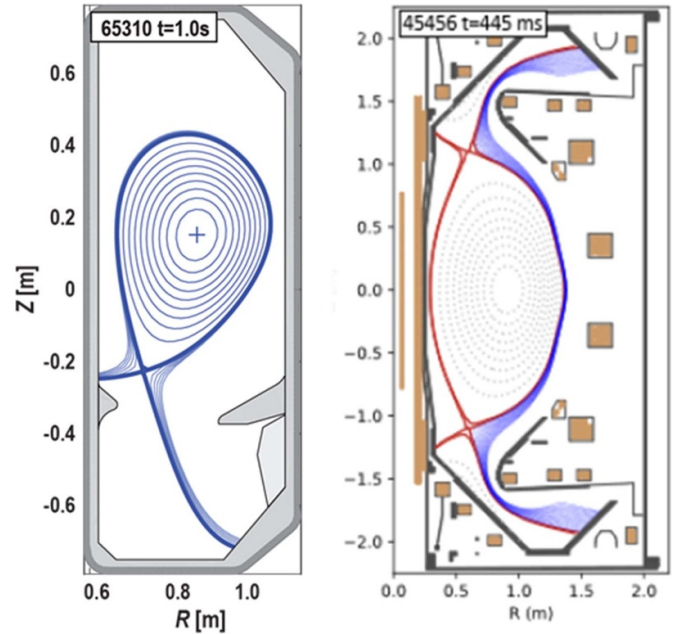

Figure 9. Long legs shapes in TCV with baffles and MAST-U respectively.

divertor configurations between a conventional and Super-X, showing that additional volume downstream of the ionisation front facilitated power and particle dissipation via plasma-neutral interactions, similarly to TCV long leg divertor experiments. In H-mode, conventional and Super-X configurations, the outer divertors are attached in the former and detached in the latter with no impact on core or pedestal confinement. A reduction in the upstream density of up to 50% at the detachment threshold was achieved in TCV and MAST-U devices using long legs divertor configurations.

Extensive comparative studies on the role played by molecular physics in detachment processes has been performed on TCV and MAST-U, both equipped with full C PFCs. On TCV [90] experimental and modelling activity probed that plasma-molecule interaction provide additional significant ion sources/sinks and power losses with respect to simple atomic process. Additional physics processes involving primarily D2+ molecules are shown to play a role during divertor detachment. Ion target flux is observed to roll-over due to both a reduction in the divertor ion source linked to an increase in Molecular Activated Recombination (MAR) which becomes significant only at sufficient low target temperature (<2.5 eV). Similar investigation has been performed as well on MAST-U in Super-X divertor [91]. Similar to TCV, MAR physics is found to play a significant role but in addition to that, further molecular processes have been identified, namely Molecular Activated Dissociation (MAD) as well electron-ion recombination (EIR) all occurring in different regions along the divertor leg accordingly to achieved temperature. Comparative investigations will be extended to metallic devices (WEST primarily) in order to assess the role, if any, of these molecular physics in devices with different PFC materials.
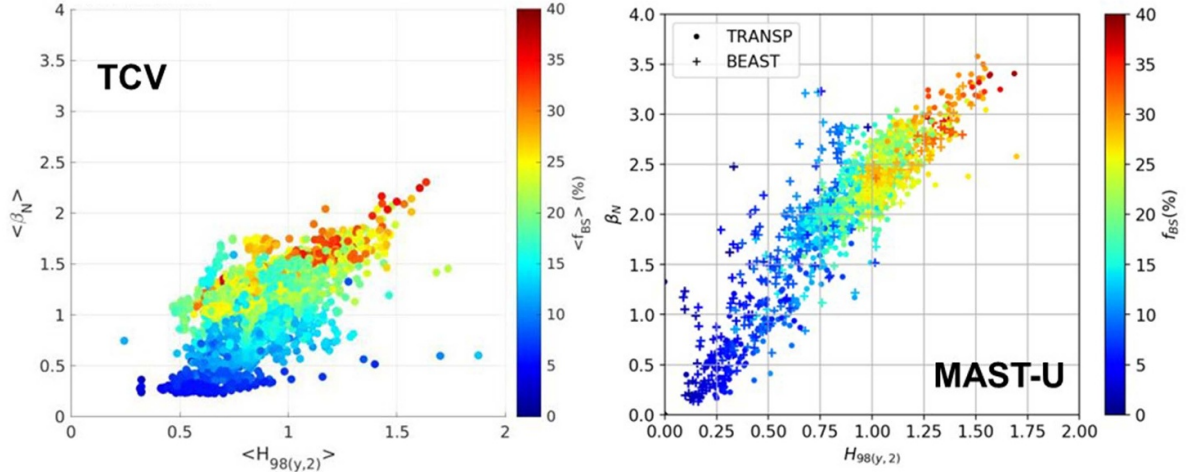
Figure 10. Development of the high β_N scenario in TCV and MAST-U: experimental database achieved with NBI on both devices (+ECRH in TCV) showing the confinement enhancement factor with colour denoting the bootstrap current fraction. Reproduced from [93] © 2024 The Author(s). Published by IOP Publishing Ltd on behalf of the IAEA. All rights reserved.

The combined experiments using the PEX upgrade in TCV and MAST-U have demonstrated the benefit of alternative divertor configuration for the control of the neutrals in the divertor area. They have also enhanced our physics knowledge about the detachment physics processes involving hydrogenic molecules and neutrals.

9. Physics and operational basis for high beta long pulse scenarios

Regarding scenario development, an effort is also currently underway within the EUROfusion TE program to explore the route towards high-β, steady-state scenarios on multiple tokamak devices. On TCV, two avenues have been explored in parallel, leveraging earlier attempts [92], with the ultimate aim of merging them into a single optimized scenario. The first avenue relies on well-established electron internal-transport barriers (eITBs) that are fully sustained in steady-state by 2nd harmonic X-mode (X2) electron-cyclotron current drive (ECCD) and bootstrap current [93], with past work bringing the bootstrap fraction up to 100%. The second avenue starts with an equally well-established H-mode regime powered by NBI, thus featuring an edge transport barrier (ETB), to which ECCD is added to increase the non-inductive current fraction. On MAST-U, routes to high β_N have been explored, within the H-mode regime, using the two available NBI sources (one on-axis and one off-axis) in the baseline double null, up-down-symmetric configuration. While the exploration of this parameter space to date is far from complete, a promising value of $\beta_N = 3.4$ was achieved transiently in MAST-U and quasi-stationary, fully non-inductive conditions with $\beta_N = 1.8$ and a 35% bootstrap current fraction were achieved in TCV [93] (figure 10). This endeavour is important to provide input to JT-60SA for a stable route towards high-β steady-state scenarios. In the next years, EUROfusion TE programme will be extended to AUG and WEST devices.

10. Physics understanding of energetics particles confinement and their interplay with thermal plasma

In TCV, a robust scenario to study NBI driven AEs and their control has successfully been developed using off-axis neutral beam power [94]. NT is shown to have major impact on observed TAE activity: TAEs appear to have a lower growth rate and amplitude in the saturated phase in NT. In MAST-U a Fast Ion Lost Detector (FILD) has also been installed and recorded its first measurements [95] characterizing the AE modes in a tight aspect ratio configuration. Using these tools, studies of fast ions losses induced by ELMs were conducted in TCV, MAST-U and AUG in different confinement regimes [96]. In TCV and MAST-U experiments performed in type-I and type-III ELMy regimes, respectively, confirm the correlation between the occurrence of ELMs and increased fast-ion losses. In addition, in low collisionality plasmas, larger increase of fast ion losses correlated with ELMs could be observed. In high collisionality plasmas, smaller increase of fast ion losses could be seen and nearly no impact on neutrons nor changes in velocity-space distribution were observed.

In addition, in AUG, a set of experiments in ELM mitigated (with resonant magnetic perturbation) plasmas have been carried out with the aim of characterizing the impact of magnetic perturbations on the confinement of beam ions. A dedicated scan in MP current suggests the presence of a threshold for the onset of fast-ion losses for the tangential beam source [97]. Simulations with the ASCOT code together with the experimental findings suggest that the effect of the MPs on ELM control could be made independent from the effect on fast-ion confinement if an appropriate arrangement of the applied MP spectrum and neutral beam sources is chosen. All these studies are bringing much better picture of the impact of ELMs (mitigated or not) to the physics of fast-ions losses in H-mode plasmas.

Fast-ions produced with neutral-beam injection (NBI) and ion cyclotron resonance frequency (ICRF) have shown their

role in relaxing the stiffness of ion heat transport in the core in the plasma core of fusion devices [98]. Recent studies in AUG have also established the role played by the ratio of ion to electron heating and that it is beneficial to keep the dominance of ion heating high in the discharge. This result is important as direct ion heating could also be favourable to increase the edge ion heat flux to enter H-mode during the initial transient phases of the ITER discharges [99]. A new ITER-relevant ICRF scenario for efficient ion heating in D-T plasmas, relying on the presence of impurities in the plasma, have been demonstrated at JET [100]. In addition, new results on the beneficial impact of MeV-range fast ions in D-T plasmas were obtained at JET [101], complementing earlier observations in the 2021 JET DT campaign [2].

Fast ions is a key ingredient in a burning plasma and the above results are giving new insights about their behaviour about ELMs, plasma shape (NT versus PT) and RMP thanks to a new set of diagnostics in TCV, MAST-U and AUG. In addition, new ICRH scenario have now been optimized and could become essential for efficient ion heating to access the burning phase in the ITER baseline scenario.

11. Conclusions & outlook

In the past 2 years, the EUROfusion coordinated experiments on several devices of different but complementary capabilities have demonstrated the benefit for answering key questions for ITER such as disruption mitigation, detachment control or the qualification of ITER grade components. Key physics questions on divertor physics, 3D effects or fast particles have also benefited from being tested in several devices with the support of modelling codes. This has also motivated the creation of subjective scientific readiness levels (SSRL) [102] to monitor the scientific progress of the Tokamak Exploitation Task Force and identify which devices have the potential to contribute to the advancement of each objective.

JET has played a very important role in the advances reported in this paper. The 2023 new DT phase aimed at developing a radiative scenario, detachment and isotopic control is essential to demonstrate these new findings in a mixed D/T plasma. In addition, the SPI has continued a dense programme in support of the ITER disruption mitigation system (DMS). With the ITER delay and JET ending, the next 10 years will have to rely even more heavily on predictive modelling to ensure the successful operation of ITER using the existing set of device (AUG, MAST-U, TCV and WEST) and the historical JET data for code benchmarking.

In the next 2 years, the TE task force will continue developing the nine lines of research presented in the introduction. With the changes to the wall material expected in ITER, special emphasize will be given to plasma operation with a full tungsten wall on topics such as conditioning by boronization, transport of tungsten from the separatrix to the core plasma, the impact of limiter operation or wall conditioning. At the same time, exploiting the recent PEX upgrade in MAST-U, TCV and WEST will carry on and include the new upper divertor [103]. The SPI installed in 2022 should

also contribute strongly to the understanding of disruption and run-away mitigation using its different capabilities (such as shattered angles) from the JET SPI. Additional ECRH power in WEST [5] is expected in 2024 and will assist the development of the long pulse H-mode in this device. In TCV [4], the amount of steerable ECRH power is also stepped up in 2024 thus enhancing the development of scenarios and their control. On its side, MAST-U will be equipped with a cryogenic pump [3] and improve its capabilities in controlling the neutrals in alternative divertor configuration. All these efforts are conducted together with development of predictive capabilities to achieve the objectives of the EUROfusion roadmap and contribute to the exploitation of ITER and the conceptual design of DEMO.

ORCID iDs

E. Joffrin ⬤ https://orcid.org/0009-0008-7527-0984
A. Kappatou ⬤ https://orcid.org/0000-0003-3341-1909
B. Labit ⬤ https://orcid.org/0000-0002-0751-8182
N. Vianello ⬤ https://orcid.org/0000-0003-4401-5346

References

[1] Zohm H. (the ASDEX Upgrade Team) 2023 *IAEA Fusion Energy Conf.* (*London, UK, 16–21 October 2023*) (available at: https://conferences.iaea.org/event/316/papers/27772/files/10438-IAEA_FEC_AUG_paper_HZohm_2023.pdf) Paper No. CN-316/1754
[2] Maggi C. *et al* 2024 *Nucl. Fusion* **64** 112012
[3] Harrison J. (the MAST-U Team) 2023 Overview of physics results from MAST Upgrade towards core-pedestal-exhaust integration *IAEA Fusion Energy Conf.* (*London, UK, 16–21 October 2023*) Paper No. CN-316/2487
[4] Duval B. (the TCV Team) 2023 Experimental Research on the TCV Tokamak *IAEA Fusion Energy Conf.* (*London, UK, 16–21 October 2023*) Paper No. CN-316/2084

[5] Bucalossi J. (the WEST Team) 2023 WEST first experiments with an ITER grade tungsten divertor *IAEA Fusion Energy Conf.* (*London, UK*, *16–21 October 2023*) Paper No. CN-316/2392

[6] Pitts R.A. *et al* 2019 *Nucl. Mater. Energy* **20** 100696

[7] Sips A.C.C. *et al* 2018 *Nucl. Fusion* **58** 126010

[8] Viezzer E. 2018 *Nucl. Fusion* **58** 115002

[9] Lehnen M. *et al* 2015 Disruptions in ITER and strategies for their control and mitigation *J. Nucl. Mater.* **463** 39

[10] Stangeby P.C. 2018 *Plasma Phys. Control. Fusion* **60** 044022

[11] Pitts R. *et al* 2011 *J. Nucl. Mater.* **415** S957–64

[12] Litaudon X. *et al* 2007 *Plasma Phys. Control. Fusion* **49** B529–50

[13] Pütterich T. *et al* 2018 The ITER baseline scenario investigated at ASDEX Upgrade *2018 IAEA Fusion Energy Conf.* (*Gandhinagar*) (EX/P8-4)

[14] Pütterich T. *et al* 2023 The stability of the H-mode entry in the ITER baseline scenario investigated in AUG and TCV *2023 IAEA Fusion Energy Conf.* (*London, UK*, *16–21 October 2023*) Paper No. CN-316/2060

[15] Sauter O. *et al* 2021 ITER baseline scenario investigations on TCV and comparison with AUG *28th IAEA Int. Conf. on Fusion Energy (virtual event, 2021)* (IAEA) (EX/P4-887)

[16] Labit B. *et al* 2024 *Plasma Phys. Control. Fusion* **66** 025016

[17] Köchl F. *et al* 2018 *Plasma Phys. Control. Fusion* **60** 074008

[18] Giroud C. *et al* 2024 *Nucl. Fusion* **64** accepted

[19] Garzotti L. *et al* 2023 *IAEA Fusion Energy Conf.* (*London, UK, 16–21 October 2023*) Paper No. CN-316/1943

[20] Marin M., Citrin J., Giroud C., Bourdelle C., Camenen Y., Garzotti L., Ho A. and Sertoli M. (JET Contributors) 2023 *Nucl. Fusion* **63** 016019

[21] Giroud C. *et al* 2023 *IAEA Fusion Energy Conf.* (*London, UK, 16–21 October 2023*) Paper No. CN-316/2322

[22] Harrer G.F. *et al* 2022 *Phys. Rev. Lett.* **129** 165001

[23] Dunne M. *et al* 2023 The quasi-continuous exhaust operational space on ASDEX Upgrade and ITER *2023 IAEA Fusion Energy Conf.* (*London, UK, 16–21 October 2023*) Paper No. CN-316/2893

[24] Radovanovic L., Dunne M., Wolfrum E., Harrer G., Faitsch M., Fischer R. and Aumayr F. 2022 *Nucl. Fusion* **62** 086004

[25] Vianello N. *et al* 2023 *IAEA Fusion Energy Conf.* (*London, UK, 16–21 October 2023*) Paper No. CN-316/1955

[26] Eich T. and Manz P. (the ASDEX Upgrade Team) 2021 *Nucl. Fusion* **61** 086017

[27] Faitsch M., Eich T., Harrer G.F., Wolfrum E., Brida D., David P., Dunne M., Gil L., Labit B. and Stroth U. 2023 *Nucl. Fusion* **63** 076013

[28] Redl A, Eich T, Vianello N and David P (the ASDEX Upgrade Team and the EUROfusion MST1 Team) 2023 *Nucl. Mater. Energy* **34** 101319

[29] Faitsch M. *et al* 2024 *26th Int. Conf. on Plasma Surface Interaction in Controlled Fusion Devices (PSI-26)* (*Marseille, France*)

[30] Gil L. *et al* 2023 Overview of EDA H-mode experiments and studies in ASDEX Upgrade *2023 IAEA Fusion Energy Conf.* (*London, UK*, *16–21 October 2023*) Paper No. CN-316/1904

[31] Hoetzl M. *et al* 2023 Non-linear MHD investigations of high-confinement regimes without type-I ELMs in ASDEX Upgrade and JT-60SA *2023 IAEA Fusion Energy Conf.* (*London, UK, 16–21 October 2023*) Paper No. CN-316/2023

[32] Sauter O. *et al* 2023 Negative triangularity tokamak operation in TCV *2023 IAEA Fusion Energy Conf.* (*London*, *16–21 October 2023*) Paper No. CN-316/1863

[33] Mariani A. *et al* 2023 Negative triangularity scenarios: from TCV and AUG experiments to DTT predictions *2023 IAEA Fusion Energy Conf.* (*London, UK*, *16–21 October 2023*) Paper No. CN-316/1703

[34] Février O. *et al* 2023 *49th European Conf. on Plasma Physics (EPS 2023)* (*Bordeaux, France*, *3 July 2023*)

[35] Heinrich P. *et al* 2023 *49th European Conf. on Plasma Physics (EPS 2023)* (*Bordeaux, France*, *3 July 2023*)

[36] Jachmich S. *et al* 2023 *49th European Conf. on Plasma Physics (EPS 2023)* (*Bordeaux, France*, *3 July 2023*)

[37] Jachmich S. *et al* 2022 *Nucl. Fusion* **62** 026012

[38] Lehnen M. *et al* 2023 Physics basis and technology development for the ITER disruption mitigation system *2023 IAEA Fusion Energy Conf.* (*London, UK, 16–21 October 2023*) Paper No. CN-316/2302

[39] Hoetzl M. *et al* 2023 Non-linear MHD modelling of transients in tokamaks: recent advances with the JOREK code *2023 IAEA Fusion Energy Conf.* (*London, UK, 16–21 October 2023*) Paper No. CN-316/1693

[40] Schwarz N. *et al* 2023 Mechanisms of the global force reduction in disruptions—experimental validation of mitigated and unmitigated VDEs with the MHD code JOREK *2023 IAEA Fusion Energy Conf.* (*London, UK, 16–21 October 2023*) Paper No. CN-316/1694

[41] Gerasimov S. *et al* 2023 VDE mitigation with SPI on JET *49th European Conf. on Plasma Physics (EPS 2023)* (*Bordeaux, France*, *3 July 2023*) p MCF90

[42] Sheikh U. *et al* 2023 *49th European Conf. on Plasma Physics (EPS 2023)* (*Bordeaux, France*, *3 July 2023*)

[43] Decker J. *et al* 2023 *Proc. IAEA Fusion Energy Conf.* (*London, UK, 16–21 October 2023*) Paper No. CN-316/2078

[44] Reux C. *et al* 2021 *Phys. Rev. Lett.* **126** 175001

[45] Reux C. *et al* 2023 *Theory and Simulation of Disruptions Workshop (TSDW), PPPL* (*Princeton, USA, 19 July 2023*)

[46] Siegling B. *et al* 2023 *49th European Conf. on Plasma Physics (EPS 2023)* (*Bordeaux, France*, *3 July 2023*)

[47] Pau A. *et al* 2022 *48th EPS Conf. on Plasma Physics (EPS)* (*Maastricht, Netherlands*, *27 June 2022*)

[48] Pau A. *et al* 2023 A modern framework to support disruption studies: the EUROfusion disruption database *2023 IAEA Fusion Energy Conf.* (*London, UK, 16–21 October 2023*) Paper No. CN-316/2057

[49] Pinches S. *et al* 2016 *26th IAEA Fusion Energy Conf.* (*Kyoto, Japan*, *17 October 2016*)

[50] Sun H.J. *et al* 2023 *Plasma Phys. Control. Fusion* **65** 095009

[51] Ricci D. 2023 *EPJ Web Conf.* **277** 02001

[52] Felici F. *et al* 2023 *IAEA Fusion Energy Conf.* (*London, UK, 16–21 October 2023*) Paper No. CN-316/2243

[53] Strait E.J. *et al* 2011 *Phys. Plasmas* **22** 021803

[54] Callen J.D. *et al* 2015 *Nucl. Fusion* **51** 094026

[55] Lehnen M.*et al* 2016 *Proc. 26th IAEA Fusion Energy Conf.* (*Kyoto, Japan*, *2016*) EX/P6-39 (available at: https://nucleus.iaea.org/sites/fusionportal/Shared%20Documents/FEC%202016/fec2016-preprints/preprint0314.pdf)

[56] Scoville J.T., La Haye R.J., Kellman A.G., Osborne T.H., Stambaugh R.D., Strait E.J. and Taylor T.S. 1991 *Nucl. Fusion* **31** 875

[57] Gambrioli M. *et al* 2023 *49th European Conf. on Plasma Physics (EPS 2023)* (*Bordeaux, France*, *6 July 2023*)

[58] Paz-Soldan C., Hu Q., Logan N.C. and Park J.-K. 2022 *Nucl. Fusion* **62** 126007

[59] Piron L. *et al* 2023 Error field detection and correction studies towards ITER operation *2023 IAEA Fusion Energy Conf.* (*London, UK, 16–21 October 2023*) Paper No. CN-316/2150

[60] Bernert M. *et al* 2023 *Nucl. Mater. Energy* **34** 101376

[61] Bernert M. et al 2022 *4th Technical Meeting on Divertor Concepts* (*Vienna*) (available at: https://conferences.iaea.org/event/286/contributions/25160/attachments/13512/21014/Bernert_IAEA_DivConcepts2022.pdf)

[62] Bernert M. *et al* 2021 *Nucl. Fusion* **61** 024001
[63] Pan O., Bernert M., Lunt T., Cavedon M., Kurzan B., Wiesen S., Wischmeier M. and Stroth U. (the ASDEX Upgrade Team) 2023 *Nucl. Fusion* **63** 016001
[64] Sun G., Reimerdes H., Theiler C., Duval B.P., Carpita M., Colandrea C. and Février O. 2023 *Nucl. Fusion* **63** 096011
[65] Henderson S. *et al* 2023 *Nucl. Fusion* **63** 086024
[66] Henderson S. *et al* 2023 *IAEA Fusion Energy Conf.* (*London, UK*, *16–21 October 2023*) Paper No. CN-316/1951
[67] Komm M. 2023 *Nucl. Fusion* **63** 126018
[68] Missirlian M. 2023 *IAEA Fusion Energy Conf.* (*London, UK, 16–21 October 2023*)) Paper No. CN-316/1989
[69] Tsitrone E. *et al* 2023 Overview of material migration and fuel retention in the full tungsten tokamak WEST after the first phase of operation *2023 IAEA Fusion Energy Conf.* (*London, UK, 16–21 October 2023*) Paper No. CN-316/1821
[70] Gunn J. *et al* 2021 *Nucl. Mater. Energy* **27** 100920
[71] Durif A., Richou M., Bergheau J. M., Corre Y., Diez M., Reilhac P., Gunn J. P. and Tsitrone E. (the WEST Team) 2023 *Fusion Eng. Des.* **188** 113441
[72] Krieger K. *et al* 2023 *Nucl. Fusion* **63** 066021
[73] Diez M. *et al* 2023 *Nucl. Mater. Energy* **34** 101399
[74] Corre Y. *et al* 2023 *Nucl. Mater. Energy* **37** 101546
[75] Aumeunier M. *et al* 2023 *IAEA Fusion Energy Conf.* (*London, UK, 16–21 October 2023*) Paper No. CN-316/1968
[76] Ratynskaia S., Paschalidis K., Krieger K., Vignitchouk L., Tolias P., Balden M., Faitsch M., Rohde V., Corre Y. and Pitts R.A. 2024 *Nucl. Fusion* **64** 036012
[77] Brezinsek S., Stamp M.F., Nishijima D., Borodin D., Devaux S., Krieger K., Marsen S., O'Mullane M., Bjoerkas C. and Kirschner A. 2014 *Nucl. Fusion* **54** 103001
[78] Borodin D. *et al* 2016 *Nucl. Mater. Energy* **9** 604–9
[79] Guillemaut C. *et al* 2017 *Nucl. Mater. Energy* **12** 234–40
[80] Zlobinski M. *et al* 2023 *IAEA Fusion Energy Conf.* (*London, UK, 16–21 October 2023*) Paper No. CN-316/2612
[81] Wauters T. *et al Nucl. Fusion* **63** 066018
[82] Wauters T. *et al* 2020 *Plasma Phys. Control. Fusion* **62** 105010
[83] Buermans J. *et al* 2022 *Proc. 48th EPS Conf. On Plasma Physics* (*Maastricht*)
[84] Wauters T. *et al Nucl. Mater. Energy* **38** 101587
[85] Hakola A. *et al* 2024 *Nucl. Fusion* **64** 096022
[86] Matveev D. *et al* 2023 *Nucl. Fusion* **63** 112014

[87] Theiler C. *et al* 2023 Effect of magnetic divertor geometry on plasma exhaust and core compatibility in TCV *2023 IAEA Fusion Energy Conf.* (*London, UK*, *16–21 October 2023*) Paper No. CN-316/1972
[88] Thornton A. *et al* 2022 *25th Int. Conf. on Plasma Surface Interaction in Controlled Fusion Devices (PSI-25)* (*Jeju, South Korea*, *12 June 2022*)
[89] Moulton D., Harrison J., Lipschultz B. and Coster D. 2017 *Plasma Phys. Control. Fusion* **59** 065011
[90] Verhaegh K. *et al* 2023 Experimental investigation of the physics & performance of the MAST-Upgrade Super-X divertor *2023 IAEA Fusion Energy Conf.* (*London, UK*, *16–21 October 2023*) Paper No. CN-316/2103
[91] Verhaegh K. 2023 *Nucl. Fusion* **63** 016014
[92] Piron C. *et al* 2019 *Nucl. Fusion* **59** 096012
[93] Coda S. *et al* 2024 Developments towards high-beta, long-pulse scenarios in TCV and MAST-U *(London, UK, 16–21 October 2023)* Paper No. CN-316-1939
[94] Oyola P. *et al* 2023 Mitigation of toroidal Alfven eigenmodes in negative triangularity plasmas at TCV *2023 IAEA Fusion Energy Conf.* (*London, UK, 16–21 October 2023*) Paper No. CN-316/2093
[95] Rivero-Rodriguez J.F. *49th European Conf. on Plasma Physics (EPS 2023)* (*Bordeaux, France*)
[96] Galdon-Quirola J. *49th European Conf. on Plasma Physics (EPS 2023)* (*Bordeaux, France*)
[97] Galdon-Quirola J. *et al* 2022 *Nucl. Fusion* **62** 096004
[98] Citrin J. and Mantica P. 2023 *Plasma Phys. Control. Fusion* **65** 033001
[99] Bilato R. R. *et al* 2023 Progresses in understanding the effects of ICRF/NBI fast-ions on core turbulence and Alfvén activity on ASDEX Upgrade *2023 IAEA Fusion Energy Conf.* (*London, UK, 16–21 October 2023*) Paper No. CN-316/1938
[100] Ye Kazakov O. *et al* 2023 *AIP Conf. Proc.* **2984** 020001
[101] Garcia J. *et al* 2023 Overview of alpha particle and fast ion studies in JET DTE2 plasmas *2023 IAEA Int. Conf. in Fusion Energy (2023)* (*London, UK, 16–21 October 2023*) Paper No. CN-316/1814
[102] Wischmeier M. *et al* 2023 Subjective scientific readiness levels (SSRL) for fusion research and their application to tokamak exploitation *2023 IAEA Fusion Energy Conf.* (*London, UK, 16–21 October 2023*) Paper No. CN-316/2290
[103] Zammuto I, Weißgerber M, Herrmann A, Dibon M, Rohde V, Schall G, Teschke M, Vierle T and Vorbrugg S (the ASDEX Upgrade Team) 2021 *Fusion Eng. Des.* **171** 112468